The Thesis Committee for Aaron Alexander Jones
Certifies that this is the approved version of the following thesis:

Microbe-Mineral Affinity in Sulfuric Acid Karst Systems

APPROVED BY
SUPERVISING COMMITTEE:

Supervisor:

Philip C. Bennett

Daniel O. Breecker

Christopher R. Omelon

Microbe-Mineral Affinity in Sulfuric Acid Karst Systems

by

Aaron Alexander Jones, B.S.Geo.Sci

Thesis

Presented to the Faculty of the Graduate School of

The University of Texas at Austin

in Partial Fulfillment

of the Requirements

for the Degree of

Master of Science in Geological Sciences

The University of Texas at Austin

August, 2011

Dedication

I dedicate this to my family, friends, and colleagues for supporting me through this process and supplying me with knowledge and encouragement when I found myself in need of either

Abstract

Microbe-Mineral Affinity in Sulfuric Acid Karst Systems

Aaron Alexander Jones, MSGeoSci

The University of Texas at Austin, 2011

Supervisor: Philip Bennett

Microbial communities influence the kinetics and pathways of reactions involved in the dissolution of a number of minerals (Ehrlich 1996). On a smaller scale these interactions can affect substrate permeability, porosity, and create highly localized biogeochemical conditions. However, a mechanistic understanding of the consequences of microbial surface colonization on calcite dissolution rate has yet to be achieved. More specifically, little is known about the impact of sulfur-oxidizing bacteria activity on the rate of carbonate mineral dissolution, or the nature of the microbe-limestone attachment and interaction. Through a series of laboratory and field experiments the effect of mineral surface colonization by microbial communities, obtained from an active sulfuric acid cave (Lower Kane Cave (LKC), Big Horn Basin, WY), on the dissolution rate of Madison Limestone was quantified. Results from laboratory experiments showed that a microbial biofilm, composed primarily of *Epsilonproteobacteria* and *Gammaproteobacteria* growing on a limestone surface oxidized thiosulfate and increased

carbonate dissolution rates up to 3.3 times faster than abiotic rates. When all thiosulfate substrate was withheld the community oxidized stored intracellular sulfur, continuing to accelerate limestone dissolution and decreasing pH. This process is sensitive to O_2 limitations.

Characterization of this aggressive sub-biofilm corrosion was more closely examined by SEM imaging. By comparing mineral surface morphology of colonized chips to non-colonized chips of various carbonate substrates, it was shown that even under conditions near equilibrium with calcite, aggressive dissolution of carbonate substratum occurs exclusively beneath the biofilm. These findings support the hypothesis that (1) sulfur-oxidizing microbial communities aggressively dissolve carbonates in order to buffer the production of excess acidity by neutrophilic communities and (2) biofilm presence affects carbonate mineral dissolution by physically separating a bulk stream water from the sub-biomat environment.

Furthermore, it was found that mineralogy affects the degree of establishment of microbial communities in this environment. Results from a series of four laboratory and one *in situ* reactor experiment showed that limestone and dolostone substratum consistently had higher biomass accumulations than silicate minerals or pure Iceland spar calcite in the same reactor. These results provide evidence to support the hypothesis that mineralogy influences microbial accumulation in sulfuric-acid karst systems. Particularly, neutrophilic sulfur-oxidizing communities accumulate in greater quantities on solid substrates that buffer metabolically-generated acidity. These results also demonstrated the dependence of microorganisms on colonization of a particular mineral

surface, possibly in order to gain access to micronutrients bound within solid substrates when exposed to nutrient-limited conditions.

Table of Contents

List of Tables

List of Figures

1 Introduction

1.1 Karst dissolution within sulfuric acid caves

Carbonate mineral dissolution kinetics, particularly calcite dissolution kinetics have been the subject of hundreds of scientific investigations (i.e. Plummer et al., 1978; Morse, 1983; Morse & Mackenzie 1990; Morse & Arvidson, 2002; Sjoeberg & Rickard, 1984; Liu & Dreybrodt, 1997). However, relatively few investigations have been conducted on microbe-mineral surface interactions (Bennett et al., 2000; Paine et al., 1933; Davis et al., 2007; Engel et al., 2004; Steinhauer et al. 2010). Advances have been made into understanding microbially-induced calcite dissolution as well as microbially-induced calcite precipitation, and their roles in cave and karst development (Dreybrodt, 1987; Ford & Williams, 1989).

Dissolution of limestone to form karst generally follows one of two models. The traditional model for speleogenesis is that carbonic acid (H_2CO_3), usually microbially-produced CO_2 in meteoric waters, dissolves limestone and forms caves. Alternatively, for karst systems where sulfide is abundant, there is the sulfuric acid speleogenesis (SAS) model. In sulfuric acid speleogenesis, chemolithoautotrophic sulfur oxidizing bacteria oxidize reduced sulfur compounds to sulfuric acid (H_2SO_4) which in turn dissolves the surrounding limestone. The mechanisms of this process are very well described in Hose et al. (2000) (see also Macalady et al., 2007; Barton & Luiszer, 2005).

Past research based on the ecosystem in Lower Kane Cave (LKC), located near Lovell, WY, concludes that the microbial community within the cave accelerates

limestone weathering (Engel et al., 2003; Steinhauer et al., 2010). This microbial community cycles sulfur and carbon across redox boundaries while generating acidity through sulfur oxidation (Steinhauer et al., 2010). The sulfur-oxidizing community in LKC is dominated by *Epsilonproteobacteria* and *Gammaproteobacteria*, however sulfate reducing *Deltaproteobacteria* are also important in this ecosystem (Engel et al., 2003). While previous SAS models have generally implicated abiotic autooxidation of sulfur with corrosion of limestone surfaces (Egemeier, 1981), mass balance calculations have shown that volatilization is only a minor contributor to oxidation and that most oxidation occurs within the microbial biomats (Engel et al., 2003). The aims of this study are to better elucidate the microbial contribution to sulfuric acid speleogenesis processes as well as the effect of carbonate mineralogy on the potential accumulation of microbial communities in sulfuric-acid karst environments.

The effect of a microbial biofilm on carbonate dissolution has been investigated previously (Steinhauer et al., 2010), whereby physical separation of the bulk media from a microenvironment beneath the biofilm is created and the sub-biofilm environment remains undersaturated with respect to calcite despite an oversaturation in the bulk media. Laboratory experiments from this study showed that pH of the biotic chamber dropped immediately after inoculation and there was a lag period of about 200 hours until the a rise in biotic dissolution rate reached steady state conditions. This pH decrease was attributed to metabolization of thiosulfate ($S_2O_3^{2-}$) to sulfuric acid upon innoculation. However, the lag between this pH decrease and dissolution rate increase was attributed to the time required for biofilm establishment on the mineral surface (Steinhauer et al.,

2010). This biofilm would then act as a semi-permeable membrane to physically separate the bulk media from the sub-biofilm environment (Wolfaardt et al. 1999).

1.2 Calcite Dissolution Kinetics

There is abundant literature regarding calcite dissolution kinetics and calcite solubility (Plummer et al., 1978; Buhmann & Dreybrodt 1985; Dreybrodt, 1981; Dreybrodt, 1987; Dreybrodt et al., 1997; Liu & Dreybrodt 1997; Morse & Berner 1974; Morse, 1983; Morse & Arvidson 2002). The Plummer-Wigley-Parkhurst model defines the solubility of calcite as fixed by temperature, PCO_2, pH, and the activity of Ca^{2+} (Plummer et al., 1978) described by three reactions that occur simultaneously:

$$CaCO_3 + H^+ \rightarrow Ca^{2+} + HCO_3^- \quad : k_1 = 10^{-4.07} \tag{1}$$

$$CaCO_3 + H_2CO_3 \rightarrow Ca^{2+} + 2HCO_3^- \quad : k_2 = 10^{-7.3} \tag{2}$$

$$CaCO_3 + CO_2 + H_2O \rightarrow Ca^{2+} + 2HCO_3^- \quad : k_3 = 10^{-10.2} \tag{3}$$

Where k_1, k_2, and k_3 represent the equilibrium constants for each equation.

Equation 1 describes the mechanism for $CaCO_3$ dissolution at low pH and low PCO_2. Equation 2 describes the mechanism at neutral pH. Equation 3 describes the mechanism at high pH and low PCO_2. This approach allows the rate of calcite dissolution to be described as simultaneously dependent on pH and dissolved CO_2 when the system is far from equilibrium with respect to calcite. Under these conditions the rate of calcite dissolution can be quantified as (Plummer et al., 1978):

$$R = k_1(H^+) + k_2(H_2CO_3) + k_3(H_2O) - k_1(Ca^{2+})(HCO_3^-) \tag{4}$$

where R is rate of dissolution that increases as saturation state (Ω) decreases. Additionally, $\Omega = IAP/K_{sp}$ where IAP is the ion activity product ($aCa^{2+} \cdot aCO_3^{2-}$) and K_{sp} is the calcite solubility product. In carbonate systems, this degree of undersaturation is generally expressed as ΔpH, where ΔpH = (equilibrium pH) – (measured pH) for a system with a given (Ca^{2+}) and PCO_2 (Morse and Berner, 1974).

Alternatively, Morse and Berner (1974) described a commonly used equation to describe the rate of carbonate mineral dissolution (Eq. 5).

$$R = -\frac{\mathrm{d}m_{\mathrm{calcite}}}{\mathrm{d}t} = \left(\frac{A}{V}k\right)(1-\Omega)^n \tag{5}$$

Where R is the rate, m is moles of calcite dissolved, t is time, A is the total surface area of the solid, V is the volume of solution, k is the rate constant, and n is the reaction order (Morse and Berner, 1974). Because mineral dissolution involves the mass transfer of a solid phase into solution, dissolution rate is commonly measured by the increase of dissolved ion concentrations in the bulk solution (in this case, Ca^{2+}). Therefore, $d[Ca^{2+}]$ can replace $m_{calcite}$ in equation (5) and $d[Ca^{2+}]/dt$ is the appearance rate of $[Ca^{2+}]$ in the bulk solution.

There is, however, a fundamental difference between the simple system just described and a sulfidic system. In the system described above, biogenic CO_2 is the source of acidity and thus dissolution kinetics depend on the interfacial transfer of atmospheric CO_2 to the system and the kinetics of the rate-limiting hydrolysis of CO_2 to H_2CO_3 (Buhmann and Dreybrodt 1985). In a sulfidic system the source of acid is HSO_4^-, and CO_2*(aq)* is a reaction by-product that diffuses away from the reacting surface. Under

the conditions anticipated for sulfuric acid speleogenesis and our experiments, low local pH near the microbe-mineral contact means the rate-determining step could be the dynamics of CO_2 or Ca^{2+} removal from the reaction area, and transport away from the interface (Steinhauer et al., 2010).

1.3 Field Site Description

Lower Kane Cave (LKC) is situated in the Bighorn River Valley, WY, USA (44°44' N, 108°11' W) (Figure 1, Figure 2). LKC is a single horizontal passage extending about 325 meters into the canyon wall, parallel to the folded core of the Little Sheep Mountain Anticline in the Madison Limestone (Stock et al., 2006). The Madison Formation is ~150–250 m thick Mississippian-age thin to medium-bedded massive grey limestone and dolomite with occasional chert and shale (Peterson 1984). Recharge water to the LKC stream is a mixture of meteoric water from Madison Limestone and slightly thermal waters (~23.5°C) from fractures in the Little Sheep Mountain Anticline (Peterson 1984). LKC is near Paleozoic oil fields which have high [H_2S] to produce sulfidic waters (Egemeier, 1981; Pearson, 2004). The locations of 3 sulfidic springs found within LKC are shown in Figure 1, where filamentous microbial mats accumulate along the outflow streams.

Microorganisms belonging to many distinct lineages within the *Proteobacteria* are associated with the these spring features that include the following Genera; *Thiothrix*, *Thiobacillus*, *Thiomonas, Thiomicrospira, Thiovulum,* and *Achromatium* (Engel et al. 2003; Engel et al. 2004). The dominant organisms in the microaerophilic stream reaches

near discharge outlets belong to lineages within the *Epsilonproteobacteria* class (Engel et al. 2003); as oxygen increases, *Thiothrix spp*. dominate the mat communities (Engel et al. 2004). Many members of these lineages are known sulfur-oxidizers.

LKC is an ideal field site because it is actively undergoing sulfuric acid speleogenesis, which form caves in carbonate rocks where either oxygen diffuses into sulfide-rich water (abiotic oxidation) or microbes oxidize sulfide (biotic oxidation) (Macalady et al., 2007). Sulfide oxidation in LKC is the result of both of these processes to produce sulfuric acid, which rapidly dissolves (Egemeier 1981; Engel et al., 2004). Carbonate rocks dissolve by the production of sulfuric acid (Eq. 6) and reactions with calcite to form gypsum (Eq. 7).

$$H_2S + 2O_2 \rightarrow H_2SO_4 \quad (6)$$

$$CaCO_3 + H_2SO_4 \rightarrow CaSO_4 + H_2CO_3 \quad (7)$$

Gypsum is very readily dissolved by the cave stream waters, resulting in removal of mass from the cave and an overall increase of the cave volume (Egemeier, 1981).

1.4 Research Questions

Environmental impacts on microbial communities are as unpredictable and imperceivable as the impact of microbial communities on the local environment. In order to gain better insight into the variables affecting carbonate mineral dissolution by sulfur-oxidizing microbial communities and the effect of mineralogy on microbial colonization by these populations the following three questions were addressed:

1) Is limestone dissolution rate impacted by the presence of the Lower Kane Cave microbial community?

2) Does mineralogy influence microbial accumulation? Specifically, do sulfur-oxidizing bacteria select carbonate mineral substrata over silicate mineral substrata?

3) Does biofilm presence affect carbonate mineral dissolution by physically separating the bulk stream water from the sub-biomat environment?

2 Materials and Methods

2.1 Field site characterization

Water and microbial samples were collected in September 2009, August 2010 and January 2011 along the Upper Spring discharge channel. Field measurements and sampling locations were chosen in accordance with previous studies (Engel et al., 2004; Steinhauer et al., 2010). Microbial biomass was collected aseptically using sterile tweezers and placed into sterile 50 ml centrifuge tubes and 2 ml cryotubes.

Water samples collected along the discharge channel were syringe-filtered through a 0.22 μm cellulose filter. Unstable parameters (temperature, pH, ORP, and specific conductance) were measured *in situ* at all sampling locations along the stream. Dissolved oxygen (DO), H_2S, and NH^{4+} concentrations were measured *in situ* using a CHEMetrics V-2000 spectrophotometer. All other chemical analyses on field-filtered water samples were conducted in the laboratory: dissolved metals were determined by ICP-MS (Agilent). Dissolved anions were determined by single-column ion chromatography (Waters). Dissolved organic carbon (DOC) and dissolved inorganic carbon (DIC) were determined using a Dohrman DC-180 carbon analyzer.

Once removed from the cave, all water samples and select microbial samples for laboratory experiments were stored at 4°C. Additional microbial samples were flash-frozen in 2 ml cryotubes in a portable liquid nitrogen dewar (for microbial characterization) before returning to The University of Texas at Austin.

2.1.1 CHARACTERIZATION OF MICROBIAL INNOCULANT

In order to determine the diversity of the LKC bacterial community, both *in situ* and in experiments (both laboratory and field continuous flow culture experiments within the Center for Disease Control (CDC) biofilm reactors (CDC 2, 3, 4, LKC CDC), microbial samples were collected for molecular identification. This biomats was aseptically sampled from the stream mat at 191 m (Figure 1) and placed into a sterilized solution composed of 1 mM Ethylenediaminetetraacetic acid (EDTA) and 0.9X phosphate-buffered saline (PBS). This solution was prepared as per Engel et al., (2004) and samples were physically disrupted by freeze-thaw (3 times, -80°C to 65°C) cycles. The sample was then further disrupted by 5 minute cycles of alternating sonication and vortexing (3X). The solution was then transferred into a sterile 15 ml centrifuge tube, spun at 5000 rpm for 10 minutes, and the supernatant removed. Genomic DNA was then extracted from biomass using an Ultraclean Microbial DNA Isolation Kit (MoBio Laboratories, Inc.; Catalog # 12224-50) and stored at -80°C until being sent to Research and Testing Laboratory in Lubbock, TX for Roche FLX and Titanium 454 next generation sequencing (http://www.researchandtesting.com/Sequencing.html). Bacterial 16S rRNA genes were amplified using the 27F/1492R primer set (Lane, 1991). Phylogenetic data was resolved down to the species level. The sequences were compared to reference sequences and designated according to percent similarity to that reference. The resulting dataset revealed both organism counts and proportional abundances of microbial groups colonizing each sample. Similar sequences were grouped as a phylotype

and used to gain further insight into both environmental and inoculant community diversity.

In order to quantify diversity for the microbial inoculant, the Simpson's Dominance index (D), the Shannon Index (H'), and Shannon Evenness (E) were computed using equations from Hill et al. (2003). Calculated values were later confirmed using EstimateS software (version 8.2, R.K. Colwell, http://viceroy.eeb.uconn.edu/EstimateS). In past studies of this nature (Engel et al., 2004) it was shown that the dominant organisms from LKC are similar in all libraries. This makes (D) a useful expression because it strongly weights dominant phylotypes, by giving the probability that two clones chosen at random will be from the same operational taxonomic unit (Hill et al., 2003). Evenness (E) is derived from (H') by calculating the ratio of (H') to the maximum possible value of (H') that could theoretically be obtained for the given community by using the total number of observed phylotypes (Hill et al., 2003). Statistical analysis was conducted at the Class level in order to better align with past data treatment (Engel et al., 2004). The results of this statistical analysis were directly compared to those from Engel et al. (2004).

2.2 Laboratory Chemostat Experiments

2.2.1 SOLID PHASE PREPARATION FOR CHEMOSTAT EXPERIMENTS

To test hypothesis (1) that limestone dissolution rate is impacted by the presence of the Lower Kane Cave microbial community, laboratory and field methods similar to those reported in Steinhauer et el. (2010) were used to compare the degree to which LKC

microbial communities enhance carbonate dissolution to previous studies. Initially, chemostat experiments were run to manipulate the environment in which SOB influence the dissolution rate of calcite. Using parallel one-liter Teflon chambers (one abiotic control, the other biotic), Madison limestone chips from LKC were selected as the experimental reactive surfaces (Figure 3, Figure 4). The chips were prepared by first crushing raw samples with a mortar and pestle and sieved to 1-2 mm in size. The chips were then sonicated in DI-H_2O for 2 hours and dipped in 0.01N H_2SO_4 for 10 seconds to remove smaller particles, and dried overnight at 100°C. Both geometric specific surface area (A_{GEO}) and reactive BET surface area (A_{BET}) (Quantachrome Autosorb-1) of the chips used in this experiment were determined in a previous study (Steinhauer et al. 2010), A_{BET} from Ar and Kr 5-point sorption curve was determined to be 0.133 m^2/g (Kr) and 0.18 m^2/g (Ar). The reactive BET surface area is approximately two orders of magnitude larger than the geometric surface area found in this study, which is consistent with previous studies (Cubillas et al. 2005; Jeschke and Dreybrodt 2002). The limestone chips were subsequently weighed to ± 0.1 mg, with 10.0012 g total mass (1.8 m^2 total A_{BET}) added to the biotic reactor and 10.0008 g total mass (1.8 m^2 total A_{BET}) added to the abiotic control reactor. The chips were placed in 850 μm pore size mesh teabags being suspended in 600 ml of experimental media solution (see below).

2.2.2 MEDIA SOLUTION PREPARATION FOR CHEMOSTAT EXPERIMENTS

The reaction solution was designed to mimic LKC cave water and prepared by equilibrating DI-H_2O water with finely powdered Iceland spar calcite. Equilibration

status, with respect to calcite, was then verified by analysis of DIC, [Ca^{2+}], pH and saturation state with respect to calcite. This solution was then filtered through a 0.2 μm cellulose filter to remove particulates. To each liter of this solution 8.3 mls of 0.1 N H_2SO_4, 0.1 g $MgSO_4$ and 0.25 g NH_4Cl was added. 9.5 liters of solution was then autoclaved at 121°C for 45 minutes before adding 20 mls and 50 mls of filter-sterilized trace metal solution and Wolfe's Vitamin solution, respectively (Burlage et al., 1998). This solution will be referred to herein as bulk media (BM).

The final prepared solution had a pH of ~6.9 and contained ~0.1 mM HCO_3^-, ~1.0 mM Ca^{2+}, with a typical Ω with respect to calcite ($\Omega_{calcite}$) of ~0.01. 600ml of this solution was transferred to a vessel to be combined with the reduced sulfur source. This input solution was pumped into both parallel reactors using a peristaltic pump at a rate of 1.2 ml/min. The reduced sulfur electron donor $S_2O_3^{2-}$ was prepared from a stock 1M solution of $Na_2S_2O_3$. This solution was filter sterilized and pumped via syringe pump at concentrations ranging from 0.67 mM 11mM into the input solution through T-fittings directly after the peristaltic pump. Magnetic stir bars constantly mixed the solution in both chambers (Figure 4).

2.2.3 SAMPLING AND ANALYSIS

The biotic chamber was inoculated with biomat collected from location 191 m in LKC (Figure 1). The pH of the biotic chamber was recorded every five minutes from 4-October through 5-November 2010 using an Omega pH probe and OM-CP-Bridge-110-10 data logger. The pH of the abiotic chamber was monitored and reported periodically

using a handheld Accumet portable pH probe. Water samples were collected 1-5 times per day from both biotic and abiotic outflow as well as the bulk media (BM) input valve. These samples were periodically analyzed for [DIC] and alkalinity. DIC was measured by injecting 250 µl of solution into a Dohrman DC-180 carbon analyzer. Total hardness was determined by EDTA titration (Eaton et al. 2005). The change in hardness over time was the result of changing [Ca^{2+}] due to dissolution. This was verified on a random selection of solution samples by ICP-MS analyses of dissolved Ca^{2+} and Mg^{2+}. Thiosulfate concentrations were measured by the Sulfite Iodometric method (Eaton et al. 2005). Microbial biomass was sampled from the reactors using sterile tweezers and examined by light microscopy (bright field and phase-contrast) using an Olympus BX41 microscope.

2.3 Laboratory Biofilm Accumulation

The CDC biofilm reactor experiments were designed to investigate biofilm accumulation and biofilm impact on carbonate mineral corrosion under a variety of conditions. To test the hypotheses that (2) mineralogy affects microbial accumulation and (3) biofilm presence affects carbonate mineral dissolution by physically separating the bulk stream water from the sub-biomat environment, continuous flow-through culture experiments with CDC biofilm reactors were used (Figure 5). Just as in the chemostat experiments described previously, the laboratory continuous flow culture experiments were designed to be analogous to the chemical conditions within LKC. Microbial

communities used in these experiments were maintained in direct contact with three different carbonate mineral substrata (Iceland spar (calcite), Madison Limestone (limestone), and Madison Dolomite (dolomite)) using a Ca^{2+}:HCO_3^-:SO_4^{2-} media that was modified by the addition of select inorganic nutrients and $S_2O_3^{2-}$ as the electron donor.

2.3.1 Solid Phase Preparation for Biofilm Experiments

The experimental mineral substrata were prepared from two main sources. Bulk mineral specimens of Iceland spar (calcite), potassium feldspar (Kspar), albite, chert, basalt, and quartz were obtained from Ward's Natural Science Establishment Incorporated. Bulk mineral specimens of unaltered Mississippian-age Upper Madison Limestone and Upper Madison Dolostone were collected from outcrop exposed along the Bighorn River near LKC. X-Ray powder diffraction (XRD) and environmental scanning electon microscope (ESEM) (FEI-Philips XL-30 TMP) XRAY analysis of these outcrop samples showed that the limestone is nearly pure calcite with minor quartz, and the dolostone is nearly pure dolomite with minor quartz. Several of the mineral coupons used for this experiment were created from the same raw material used in a previous study (Bennett et al., 2001). Trace element analysis of the following coupon materials are presented in Table 1: quartz, Kspar (plagioclase), basalt, and albite (oligoclase).

All samples except the Iceland spar calcite were cored with a 1 cm diameter diamond coring bit on a drill press, cut to ~2 mm thickness on a diamond saw, and polished using thin section preparation techniques to match the dimensions necessary to fit the CDC reactor rods. The coupon holders accommodate three 1/2 inch (12.7 mm)

diameter coupons each. Iceland spar calcite was prepared to the same specifications by first fracturing the samples to the correct thickness with a razor blade and then hand polishing the samples with 600 grit sandpaper to the correct diameter and circular shape. Scanning electron microscope (SEM) examination of all starting material specimens was then conducted for comparison with coupons run through the experimental processes.

The CDC Biofilm Reactor consists of eight (8) polypropylene coupon holders suspended from a UHMW-polyethylene ported lid. The lid with coupon holders and coupons is mounted in a 1-liter glass vessel with side-arm discharge port (Figure 5). A liquid media (described herein) was circulated through the vessel while mixing and shear was generated by a magnetic stir vane rotated by a magnetic stir plate at 115 RPM. Sampling of the coupons was conducted by aseptically removing individual coupon holders with suspended coupons.

2.3.2 Laboratory Biofilm Media Preparation

Media preparation for the CDC biofilm reactor experiments was nearly identical to that of the chemostat experiments. The only chemical difference was variable amounts of H_2SO_4 were added to the media to achieve desired pH values. For a more complete description of the components of this media see section 2.2.2. The input solution was pumped through the CDC reactor at 1.2 ml/min, with $S_2O_3^{2-}$ as the reduced sulfur substrate. The reduced sulfur substrate is a stock 1M solution of $Na_2S_2O_3$. This solution was filter sterilized and mixed via syringe pump at 0.002 ml/min into the input solution.

Reaction volume was held constant at 400 ml, and the outflow tubing was outfitted with a glass bubble trap to ensure no microbial contamination from drainage.

Mineral coupons were rinsed several times with input solution to remove debris and the entire apparatus was autoclaved at 121^{o}C for 45 minutes. Select chips were retrieved for imaging on a FEI-Philips XL-30 TMP SEM following previously published methods for chemical critical point drying (Bennett et al., 2006). Select chips were also processed by 3, 5 minute cycles of alternating sonication and vortexing in a calcite equilibrated 2% tween 20 solution to remove the biomass. Wet weight, dry weight, and post biomass removal weights were recorded for quantification of dry biomass accumulation per unit surface area.

2.3.3 Field Biofilm Experiments

In January of 2011 a CDC biofilm reactor was taken into LKC. Solid-phase mineral preparation for the field continuous flow culture experiments was identical to preparation for laboratory experiments. This was done in order to test if the results of similar laboratory experiments hold true *in situ*. Upper Spring cave stream water was used as the input media for the reactor and was pumped continuously for 7 days (from 19-Jan through 26-Jan) from 191 meters from the back of the cave (Table 4, Table 5). This location is approximately 4 meters downstream from the Upper Spring source waters. All components, mineral coupons, and tubing were sterilized by autoclave at 121°C for 45 minutes prior to deployment. Initially, 400 ml of 0.2 μm filtered cave water was pumped into the reactor. The chamber was then inoculated with cave 191 m biomat

and stirred for 24 hours to allow for growth of microorganisms within the reactor. At 24 hours the pump was turned on and LKC water added to the chamber at a flow rate of 60 ml/min through a 0.45 μm filter. This was the slowest that the pump would run continuously without halting.

After 7 days, the coupons were removed and placed into sterile 15 ml centrifuge tubes prefilled with 0.2 μm filtered cave water from 191 meters. All field instruments that came in contact with the mineral coupons were sterilized between each chip removal. Select mineral coupons were then prepared for imaging by SEM as described previously.

2.3.4 BIOFILM EXPERIMENTAL VARIATIONS

Five separate laboratory reactor experiments were run under identical input media conditions, with initial pH being the only altered variable CDC 1, CDC 2, and CDC 3 were all run at a pH of 6.6. CDC 4 was conducted at a pH of 8.3 in equilibrium with calcite in order to investigate the impact of biofilm development on carbonate corrosion under equilibrium conditions.

CDC 1 was the only reactor in which the microbial inoculant was a pure culture, *Thiothrix unzii* (ATCC type strain 49747). *Thiothrix unzii* is a colorless, filamentous, neutrophilic, chemoautotrophic, sulfur-oxidizing member of the *Gammaproteobacteria* class that is known to use both sulfide and thiosulfate as sulfur sources and have the ability to store sulfur intracellularly (Howarth et al., 1999). *Thiothrix unzii* is closely related to *Thiothrix spp.* that is known to dominate the biomats community within LKC (Engel et al., 2004). CDC 2, CDC 3, CDC 4, and LKC CDC were all inoculated with an

aliquot of biomats aseptically collected from the 191m position of the LKC upper stream. This inoculant was sequenced in order to determine phylogeny.

3 Results

3.1 LKC Geochemistry

Geochemical data (major constituents) for stream water gathered in 2010 are presented in Table 2. The same trends in major constituents are observable in 2010 as in 2011. Although the pH values measured in 2010 are lower than those in 2011 these values follow the same general trend to increase downstream of the spring source. Minor chemical constituents for 2010 are presented in Table 3.

Geochemical data (major constituents) for stream water within LKC in January 2011 are summarized in Table 4. Water temperature remains steady ($21.8 \pm 0.1^{\circ}C$). pH increases slightly along the flow path from 7.28 to 7.42. Dissolved oxygen increases from 0.27 ppm at the upper spring outlet (191 m) to 1.5 ppm (205m). Sulfate concentrations generally increase from 1.14 mM to 1.28 mM along the Upper Spring transect. At the Lower Spring (248 m) the sulfate concentration is 1.15 mM increasing to 1.17 mM at 249 m. Calcium increases slightly along the upper spring transect as well (1.34 mM to 1.71 mM). Other cations and minor chemical constituents showed no major trends along the transect. Minor constituents for 2011 are presented in Table 5. The Ω value reveals that the stream water is near equilibrium with or slightly supersaturated with respect to calcite at all points along the stream.

3.2 Laboratory Dissolution Rate

3.2.1 ABIOTIC DISSOLUTION RATE

The first measured dissolution rate for the abiotic chemostat using [Ca^{2+}], flow rate, and the geometric surface area (R_{GEO}) was 8.85×10^{-11} mol·cm^{-2}·s^{-1} at a measured pH of 8.2 at 40:50 (Table 6). In contrast, the bulk media feeding the abiotic chamber had a pH of 6.9. Within the first 12 hours of experimental startup, the pH went from 6.9 to about 8.2. The abiotic dissolution rate reached a maximum of 9.24×10^{-11} mol·cm^{-2}·s^{-1} at pH 8.04 after 261 hours and a minimum of 5.60×10^{-11} mol·cm^{-2}·s^{-1} at pH 7.8 after 405 hours.

After approximately 12 hours, the abiotic dissolution rate remained fairly constant and flow rate was maintained at 1.21 ml/min. This flow rate gave a residence time of about 8.3 hours. The mean pH was 8.02 ± 0.14, consistent with water slightly out of equilibrium with calcite and atmospheric CO_2.

Abiotic autooxidation of ~67% of $S_2O_3^{2-}$ occurred only during the portion of the experiment when $S_2O_3^{2-}$ concentration was ~11 mM (Table 8). Loss of $S_2O_3^{2-}$ due to autooxidation was not detectable in the portions of the experiment at and below [$S_2O_3^{2-}$] 4.13 mM. There was, however, a notable change in pH when the thiosulfate concentration was changed (Figure 6). In particular, pH decreased to from ~8.2 to ~7.8 ± 0.1 from hour 335 through the remainder of the experiment when thiosulfate concentration was reduced from 4.13 mM to 0.89 mM. This pH change is not explained here, but was not accompanied by a notable change in [Ca^{2+}] or [DIC] (Table 6). This same phenomenon was not understood in a previous study (Steinhauer et al. 2010). [Ca^{2+}]

in the abiotic reactor remained relatively constant no matter how much thiosulfate was present, with a mean concentration of ~1.67 mM ± 0.1. The mean dissolution rate (R_{GEO}) over a 428-hour period derived from the $\Delta[Ca^{2+}]$ ($[Ca^{2+}]_{out}-[Ca^{2+}]_{in}$) and flow rate (1.21 ml/min) was 7.46×10^{-11} $mol \cdot cm^{-2} \cdot s^{-1}$ ± 0.5. SO_4^{2-} measured periodically during this experiment showed very little abiotic production of sulfate (0.11 mM to 0.21 mM) (Table 8).

3.2.2 BIOTIC LABORATORY DISSOLUTION RATE

Effect of $S_2O_3^{2-}$ concentration on biotic pH

The initial conditions in the biotic reactor were identical to the abiotic reactor but quickly changed after inoculation with microbial biomass from LKC. pH increased to a maximum value of 9.2 and held steady until air was introduced at a rate of 2 ml/min at hour 48. After the introduction of air, pH decreased steadily from 9.2 to 8.57 after 62 hours. At hour 132 the thiosulfate concentration was decreased from 11 mM to 0 mM, followed 2 hours later by a rapid decrease in pH to 6.78 that leveled off at hour 152 (Figure 6). At hour 161, $S_2O_3^{2-}$ was reintroduced at a concentration of 11 mM, and after a small spike in pH, the pH continued to drop steadily. At hour 230, $S_2O_3^{2-}$ was dropped to 4.13mM which led to a very small decrease in pH; only 6% of the thiosulfate was removed from the biotic system while there was no abiotic removal. At hour 263 the $S_2O_3^{2-}$ concentration was changed to 0.89 mM: there was an immediate small spike in pH, which then decreased to a new minimum of 5.5 at hour 333.

Effect of O_2

For the duration of the experiments, ~75% of thiosulfate was being removed from the biotic chamber while none of the thiosulfate was removed by abiotic processes (Table 8). At hour 340 the air inlet was shut. Immediately after this the biotic pH started to increase until it reached a local maximum of 6.4 at hour 390. At ~393 hours air was reintroduced at a rate of 2.0 ml/min. There was an immediate drop in pH as a response to the reintroduction of oxygen from 6.4 to 6.2 at ~430 hours. This abrupt pH response to O_2 is contradictory to the findings by Steinhauer et al. (2010), which found that changes in O_2 concentration had very little (if any) affect on pH of the biotic chemostat (Steinhauer et al., 2010).

Dissolution rate in biotic chamber

During the first 90 hours of the experiment, measured [Ca^{2+}] in the biotic chamber was lower than that in the abiotic chamber (Table 7). The biotic dissolution rate was on average about 57% lower than the abiotic with a value 4.4 x 10^{-11} mol·cm^{-2}·s^{-1} ± 0.5 compared to the average abiotic dissolution rate of 7.7 x 10^{-11} mol·cm^{-2}·s^{-1}. However, after the pH decrease at hour 134 the rate of dissolution in the biotic chamber exceeded that of the abiotic chamber. Prior to hour ~134 abiotic dissolution rate was higher than biotic (Table 7, Figure 6). For the duration of the experiment the pH remained lower and the dissolution rate remained higher than the abiotic chamber.

During the time period when $S_2O_3^{2-}$ concentration was 4.13 mM (hours 230-263) the average biotic dissolution rate is on average 2.3 X that of the abiotic chamber, with

rates of 1.8 x 10^{-10} mol·cm^{-2}·s^{-1} and 7.9 x 10^{-11} mol·cm^{-2}·s^{-1}, respectively. During this same period there was no abiotic thiosulfate oxidation and biotic oxidation was only 0.03 mM/hr, or 6% of input concentration (Table 8). Once the thiosulfate concentration was reduced to 0.89 mM (hour 333) the biotic dissolution rate was on average 2.9 X greater than the abiotic dissolution rate (1.9 x 10^{-10} mol·cm^{-2}·s^{-1} vs. 6.5 x 10^{-11} mol·cm^{-2}·s^{-1} respectively). During this period there was again no abiotic oxidation of thiosulfate whereas biotic oxidation was stable at 75% of input concentration at a rate of 0.08 mM/hr. At several points during the experiment the biotic dissolution rate was as high as 3.3 times that of the abiotic dissolution rate (Figure 6). Microbial biomass was then sampled from the reactors using sterile tweezers and examined by light microscopy (Figure 7). The resulting light images revealed globules within cells interpreted as intracellular sulfur deposits in previous studies (Engel et al., 2004; Steinhauer 2010). Microbial accumulation on "teabags" containing the limestone chips was also evident upon retrieval from the chambers (Figure 8).

Sulfate concentrations in the biotic chamber were much higher and were generated at a faster rate than that in the abiotic chamber. The input media had [SO_4^{2-}] of 1.35 mM. At hour ~334, the [SO_4^{2-}] concentration in the biotic chamber was 3.89 mM while the abiotic reactor had increased only slightly to 1.56 mM (Table 8). Sulfate was generated at 0.28 $^{\pm}$ 0.03 mM/hr in the biotic chamber. While consuming 0.67 mM $S_2O_3^{2-}$ the abiotic reactor generated 2.54 mM sulfate by autooxidation (Table 8). This consumption ratio was fairly consistent for the duration of the experiment. The abiotic

reactor continued to consume about 0.22 mM (0.03 mM/hr) thiosulfate while generating between 0.11 mM and 0.21 mM sulfate (0.02 $^{\pm}$ 0.01 mM/hr) (Table 8).

3.3 Laboratory Biomass Accumulation

3.3.1 CARBONATE MINERAL COUPON ACCUMULATION

Four laboratory reactors with identical mineral coupons, bulk media chemistry, flow rate and thiosulfate concentrations were used to test whether more biofilm accumulated on one substratum when given the opportunity to colonize a variety of carbonate substratum. All laboratory CDC reactor experiments were conducted over a period of 3 weeks and are summarized in Table 9 as the mean value of three chips of each mineral type. Dry weight of biofilm accumulated on the carbonate coupons used in the CDC reactor experiments were measured by the methods mentioned in the Methods section.

Experiment CDC 1 was inoculated with a pure culture of *Thiothrix unzii* (ATCC type strain 49747). After three weeks, dolostone had the highest accumulation with an average dry mass of 25.9 mg/cm^2 compared to limestone (14.4 mg/cm^2) and calcite (2.3 mg/cm^2). Biofilm accumulation was consistently highest on limestone and dolostone in all of the mixed culture experiments despite varying being in solutions with different pH conditions (6.6 or 8.3).

In addition to the 4 laboratory reactor experiments, one reactor experiment was run in LKC for one week; results show that dolostone accumulated a mean dry mass of

biofilm 5.3 mg/cm^2, limestone accumulated 4.9 g/cm^2, while calcite accumulated 2.3 mg/cm^2 (Table 9).

3.3.2 SILICATE MINERAL COUPON ACCUMULATION

Dry mass accumulation values on the silicates were consistently and significantly lower than measured values for the carbonate mineral coupons (Table 9). Samples left in the abiotic chamber for three weeks showed no biomass accumulation, examined by SEM with media identical to CDC 1, CDC 2, and CDC 3 are shown in Figure 10..

One surprising result from the CDC reactors 2, 3, and 4 was that basalt accumulated more biomass than calcite in every experiment with a mean dry biomass of 6.0 mg/cm^2. Other than basalt, quartz accumulated the most biofilm mass of the silicates with a mean accumulation of 2.2 mg/cm^2. Chert and potassium-feldspar accumulated the least mass with mean values of 0.5 mg/cm^2. SEM images of the silicate mineral coupons confirm that minimal accumulation indeed takes place (Figure 12).

SEM images after 3 weeks in CDC 1 inoculated with a pure culture of *Thiothrix unzii* (Figure 11) reveal vast differences in biomass accumulation between mineral types. Kspar, Basalt, and quartz mineral chips all exhibit homogeneous distribution of *Thiothrix unzii* filaments (Figure 11 A, D, & E). Albite and chert are very sparsely covered with filaments (Figure 11 B, C). Basalt, in particular, has a very dense "web" of *Thiothrix unzii* filaments homogeneously coating the entire mineral surface (Figure 11D).

SEM images taken after the mineral coupons were left for 3 weeks in CDC 2 inoculated with a Lower Kane Cave mixed culture (Figure 12) reveal greater differences

in microbial colonization. The basalt surface is the only silicate coupon that had substantial accumulations of filamentous microorganisms (Figure 12D). All other silicate mineral surfaces seem to be covered completely by non-filamentous bacteria, possibly coated in extracellular polysaccharides (EPS) (Figure 12 A, B, C, & E).

3.4 Mineral Etching

Abiotic and biotic dissolution of carbonate substrata were also analyzed by SEM, revealing distinct morphological differences between dissolution textures with no biomass accumulation and those with biofilm development. Iceland spar calcite, Madison Limestone, and Madison Dolostone show relatively smooth surfaces after solid phase preparation (but prior deployment within the reactor), totally free of bacterial filaments (Figure 13). After three weeks in the abiotic CDC reactor at a pH of 6.6, subsequent analysis shows no obvious signs of mineral corrosion (Figure 14). Similarly, after three weeks in an abiotic CDC reactor at a pH of 8.3, analysis by SEM shows no obvious signs of mineral corrosion (data not shown).

After 3 weeks in CDC 1, SEM analysis of the calcite substrate reveals "spiky" corrosion features (Figure 15), with abundant accumulation of *Thiothrix unzii* filaments in patches on the mineral surface. Each of the individual spikes appears to be coated with EPS with individual filaments extending from the tip of each spike (Figure 15 C, D). This type of corrosion has been documented in past studies (Jones et al., 2008) and is indicative of biofilm presence on a carbonate surface.

After 3 weeks in CDC 1, both limestone and dolostone surfaces were deeply corroded (Figure 16). Both substrates were almost completely covered by microbial filaments of *Thiothrix unzii*, leaving very little of the substrate surface exposed. In regions where the substrate surface was observable through the tangled filaments, the carbonate surfaces appear aggressively corroded (Figure 17). Similar results were found in experiment CDC 2 (Figure 18 and Figure 19). Figure 18A shows coverage of the mineral surface by a mixture of filamentous and rod shaped bacteria. Partial removal of the mixed culture biofilm by brief immersion in calcite-equilibrated tween 20 solution reveals the deep corrosion that took place in the sub-biofilm environment (Figure 18B and Figure 19).

After 3 weeks in CDC 4, calcite had similar corrosion features to those in CDC 1, despite a maintained pH of 8.3 in the bulk solution (Figure 20). The "spikes" on calcite in the neutral reactor were less uniform than those in CDC 1. In regions where biofilm coverage is less substantial, corrosion features appear to follow the contours of individual filaments (Figure 21). These grooves do not follow cleavage plains as in the abiotic experiments, but instead curve and follow arced patterns as filaments would. Most of these grooves are filled with very small spikes (<500 nm). In this reactor, dissolution appears to be limited to regions colonized by microbial populations.

After 3 weeks in CDC 4, Madison Limestone and Madison Dolostone had deep corrosion features (Figure 22, Figure 24). Images of Madison Limestone and Madison Dolostone reveal full coverage of biofilm on the surface, except in areas where the biofilm had peeled away from the substrate surface during drying (Figure 22A, Figure

24A). At greater magnification of regions where the bare mineral surface is visible, the surface is extremely etched and pitted (Figure 22B, Figure 24B). Greater magnification of the biofilm over the limestone surface reveals a relatively homogenously smooth biofilm surface with intermittent bacterial filaments (Figure 23). This contrasts greatly with the thick, intertwined bacterial filaments composing the biofilm of both CDC 1 and CDC 2. Between the intermittent filaments is a smooth surface that appears to be EPS composed of singular microorganisms. All of the previous observations for Madison Limestone in CDC 4 can be applied to Madison Dolostone in CDC 4 as they are virtually identical. The aggressiveness and extent of the pitting and corrosion of these carbonate surfaces appears to be as substantial as CDC 1 and CDC 2.

After 1 week in LKC, LKC CDC calcite showed similar corrosion features to those in CDC 1, CDC 2, and CDC 4 (Figure 25). The spiky corrosion features resulting from the LKC CDC experiment were much less extensive than those in any other CDC experiment described herein, and while the individual spikes also do not appear to have the individual filaments extending from their tips as in CDC 1, the surface does appear to be covered by a thin cover of EPS. Accumulated microbial biomass appears to be primarily filamentous in morphology. Filament coverage is patchy as in CDC 1.

Madison Limestone and Madison Dolostone within LKC CDC did not show similar corrosion features as found in CDC 1, CDC 2, and CDC 4 (Figure 26, Figure 27). Images of the biofilm over both surfaces reveal a web of intertwined bacterial filaments (Figure 26A, Figure 27). While this microbial biofilm does not appear to be that different from those in laboratory experiments, upon greater magnification, the surface is more

dominated by filamentous microorganisms in the field experiment than in the laboratory. Greater magnification reveals little to no corrosion of the limestone surface and possible slight corrosion of the dolostone surface (Figure 26A, Figure 27B).

3.5 16S rRNA at 191m Statistical Analysis

Further phylogenetic analysis reveals that a majority of the microbes come from two main phylotypes (Table 10). Analysis of this phylogenetic data reveals two dominant classes within the inoculant that represent ~98.38% of the total counts (Table 10, Table 11). *Epsilonproteobacteria* represents ~54.79% and *Gammaproteobacteria* was found to represent ~43.59% of the community. *Deltaproteobacteria* represent only ~0.43% of the community. The remainder of the representative classes are presented in Table 10.

Analysis of this phylogenetic data reveals two dominant genera within the inoculant that represent ~97.42% of the community (Table 12, Table 13). These most abundant genera are *Sulfurovum* (~53.84%) and *Thiothrix* (~43.57%). *Sulfurospirillum* is the next most abundant genus representing ~0.41% of the microbial community (Table 12). The remainder of the representative genera show counts that compose <0.4% of the total community (Table 12).

The Shannon-Wiener (H'), Simpson's (D), and evenness (E) indices were calculated for 16S rRNA of the microbial inoculant from 191m along the LKC stream.

At the class level I calculated an H' of 0.79, (E) of 0.27, and a (D) of 0.49 (Table 14). At the genus level I calculated an H' of 0.87, (E) of 0.23, and a (D) of 0.48 (Table 14).

4 Discussion

4.1 Role of $S_2O_3^{2-}$ and S^0 in metabolism and Limestone Dissolution

The Madison Limestone dissolution rate in the biotic chamber reached about 3.3 times the rate in the abiotic chamber using thiosulfate as the electron donor (Figure 6). Consistently lower output solution concentrations of thiosulfate from the biotic chamber support this data (Table 8). The microbial mats within LKC are up to 50% elemental sulfur by weight (Mabin, K., 2005). Therefore, it is important to note that while the microbiology and biogeochemistry of a sulfidic system is complex, a few reactions illustrate the effect of the oxidation (both biotic and abiotic) of sulfur compounds on limestone dissolution in non-photosynthesizing environments. These reactions are (Kelly, 1999):

$$H_2S + 2O_2 \rightarrow SO_4^{2}- + 2H^+ \qquad \Delta G = -714 \text{ KJ/mol} \qquad (8)$$

$$HS^- + 0.5O_2 \rightarrow S^0 + OH^- \qquad \Delta G = -145 \text{ KJ/mol} \qquad (9)$$

$$S^0 + H_2O + 1.5O_2 \rightarrow SO_4^{2-} + 2H^+ \qquad \Delta G = -507 \text{ KJ/mol} \qquad (10)$$

$$S_2O_3^{2-} + H_2O + 2O_2 \rightarrow 2SO_4^{2-} + 2H^+ \qquad \Delta G = -739 \text{ KJ/mol} \qquad (11)$$

$$S_2O_3^{2-} \leftrightarrow S^0 + SO_3^{2-} \qquad \Delta G = +26.8 \text{ KJ/mol} \qquad (12)$$

Abiotic autooxidation of H_2S (Eq. 8) is a second order reaction that is spontaneous in aerobic aqueous systems (Millero et al., 1987). While work still needs to be conducted on the mechanisms of biologic sulfur oxidation, it is known that members

of the same genus as *T. unzii* oxidize both sulfide and S^0 all the way to sulfate (Eq. 8 & 10). Other SOB partially oxidize sulfide and store the resulting S^0 internally (Eq. 9) where it can later be oxidized (Eq. 10) in times of low sulfide availability (Ehrlich, 1996; Strohl and Schmidt, 1984). Members of this genus were shown to be present in the inoculant used in this experiment (Table 12). Recent studies have found that SOB may catalyze and accelerate sulfide oxidation even at low oxygen concentrations which accelerates cave formation (e.g. Engel et al., 2004; Steinhauer et al., 2010). This process can be represented by equation (13) for the sulfidic system in question and equation (14) which represents general oxidation by chemoorganotrophic SOB in disoxic environments (Thamdrupet al., 1993). Microbial populations that catalyze sulfur oxidation to sulfate (Eq. 14) will then increase the rate of SAS suggested by Egemeier (1981) (Eq. 13). Note that equation (13) is an overall equation combining Eqs.6 & 7.

$$H^+ + HSO_4^-{}_{(aq)} + CaCO_3{}_{(s)} + H_2O{}_{(l)} \rightarrow CaSO_4 + H_2O{}_{(s)} + CO_2{}_{(g)} \quad (13)$$

$$4S^0 + 4H_2O \rightarrow SO_4^{2-} + 3H_2S + 2H^+ \quad (14)$$

Chemolithoautotrophic SOB obtain energy from oxidation of reduced inorganic and organic sulfur compounds such as sulfide, thiosulfate, polythionic acids, thiocyanate, carbon disulfide, carbonyl sulfide and methylated sulfur compounds (Kelly, 1982, 1988). Sulfur oxidation generates NAD(P)H and ATP. CO_2 reduction in the Calvin Cycle is dependent on the electrons provided by sulfur oxidation. In turn, the H^+ generated by

sulfur oxidation can be used to regenerate NAD(P)H for the reductive part of the Calvin Cycle (Kelly, 1999).

Microorganisms in LKC are known to take advantage of sulfur in its various redox states and compounds (Engel et. al., 2005). The Madison Limestone dissolution rate in the biotic chamber reached about 3.3 times the rate in the abiotic chamber by using thiosulfate as an electron donor (Figure 6). This suggests that the chemoautotrophic bacteria are utilizing thiosulfate as an energy source while generating acidity and sulfate as described by equation (11), generating a significant amount of energy (Kelly 1999). The introduction of air (hour 48) showed the dependency of the microbial communities on oxygen to generate this acidity. The initial pH increase was due to a switch of conditions from aerobic to anaerobic directly after inoculation. In contrast, any thiosulfate consumed in the abiotic reactor would tend to follow the pathway described in equation (12) which does not generate acidity (Kelly 1999). This explains why the pH remains relatively constant in the abiotic reactor (Table 6, Figure 6).

The biotic dissolution rate was erratic, but appeared to coincide with changes in thiosulfate concentration (Figure 6). The small upward spikes in pH that occur immediately after these changes likely reflect short lags in microbial metabolism as the community readjusts to new electron donor concentrations.

From hours 134-152 no thiosulfate was provided to the already established microbial community (Figure 6). The drop in pH (~8.5 → ~6.8) is accompanied by a proportional increase in dissolution rate (Figure 6). This enhanced calcite dissolution is likely due to the microbial population generating acid from stored intracellular S^0 (Eq.

10). Occasional examination of microbial filaments by light microscopy during this experiment confirms their ability to store intracellular S^0 (Figure 7).

SOB require O_2 in order to generate acid by equation (11) from thiosulfate or equation (10) from intracellular S^0. The rapid change in dissolution dynamics around hour 134 suggests that the microorganisms were not generating substantial acidity prior to this time. In fact, one unique phenomenon that was observed in this experiment was the sensitivity of pH to oxygen supply: the initial pH increase to ~9.2 is likely due to imposed anoxia in the biotic reactor as a result of the magnitude of initial microbial inoculant.

As noted earlier, any time that the air supply was removed from the biotic chamber, there was an immediate increase in pH. The consumption of thiosulfate during this period (Table 8) indicates that the microorganisms were sequestering thiosulfate as intracellular S^0 according to equation (12). This reaction does not generate acidity and thus would not aid in limestone corrosion. For this period of the experiment the accumulating biofilm actually serves as a diffusion boundary which slows the limestone dissolution rate to below abiotic rates (Figure 6).

Inhibition of mineral dissolution due to the presence of biofilm has been suggested in previous studies where binding of EPS to the mineral surface inhibits dissolution pit formation (Luttge and Conrad 2004; Luttge et al., 2005; Welch et al., 1999, Steinhauer et al., 2010). Under these circumstances, the biofilm serves as a semi-permeable barrier, limiting the access of distally generated H^+ to the limestone surface and restricting diffusion of Ca^{2+} away from the sub-biofilm microenvironment into bulk

solution (Luttge et al., 2005). Once air was pumped into the chamber and the pressure of anoxia was removed, the pH immediately began to decrease as the SOB began to generate acidity (Figure 6).

The sensitivity of pH in the biotic chamber to changes in thiosulfate concentration are further emphasized by the reduction in thiosulfate concentration from 4.13 mM to 0.89 mM at hour 333 (Figure 6), where an immediate increase in dissolution rate upon decreasing the thiosulfate concentration was observed. Prior to this change the biotic dissolution rate was on average 2.9 times that of the abiotic chamber with (1.9×10^{-10} $mol \cdot cm^{-2} \cdot s^{-1}$ vs. 6.5×10^{-11} $mol \cdot cm^{-2} \cdot s^{-1}$, respectively). After this change in thiosulfate concentration there was no abiotic oxidation of thiosulfate and biotic oxidation was stable at 0.08 mM/hr. As noted previously, at several points during this experiment the biotic dissolution rate reached values of 3.3 times that of abiotic dissolution.

It is likely that this decrease in pH at hour 333 results from a similar mechanism as that initiated by no thiosulfate being present in the media. Once thiosulfate decreased it became a limiting component and a fraction of SOB began to oxidize S^0 and generating acidity according to equation (10). This hypothesis is supported by the stoichiometry of these reactions: according to equation (11), 2 moles of sulfate would be generated for every mole of thiosulfate consumed. However, the microbes in this experiment are generating about 3.4 moles of sulfate for every mole of thiosulfate consumed (Table 8). In order account for this excess sulfate generation and the corresponding decrease in pH, some intracellularly-stored S^0 needs to be oxidized according to equation (12).

4.2 16S rRNA at 191m

Spatially, the closest samples with statistical analysis of phylogenetic data calculated in Engel (2004) were of filamentous biomat located at 190 m and 195 m. The Shannon-Wiener (H'), Simpson's (D), and evenness (E) indices were thus compared to those calculated for 190 m and 195 m (Table 14).

When comparing (H'), (E), and (D) at LKC 191 m to those indices calculated for 190 m in 2004, it was found that the phylotype distribution of the inoculant is statistically less diverse (lower H'), less evenly distributed (lower E), and has about equivalent dominance of relatively few phylotypes (equivalent D) (Table 14). At the class level H' was 0.79, which is much lower than the H' at 190 m (1.36) and 195 m (1.24). The (E) of 191 m was 0.27 at the class level compared to 190 m (0.39) and 195 m (0.54). The (D) of 191 m (0.49) was in between the values for 190 m (0.65) and 195 m (0.38). This statistical analysis is confirmed by further phylogenetic analysis, which reveals that a majority of the counts come from two main phylotypes (Table 10). This is important as these two dominant classes are known to contain mostly sulfur-oxidizing microorganisms.

Analysis of this phylogenetic data reveals two dominant classes within the inoculant that represent ~98.38% of the total counts (Table 10, Table 11). The most abundant class is *Epsilonproteobacteria*, which represents ~54.79% of the total counts. *Epsilonproteobacteria* have recently been recognized as important filamentous, sulfur-oxidizing members of deep-sea hydrothermal vent communities (Campbell et al., 2006).

Previous investigations at LKC also found that the sulfur-oxidizing community is dominated by *Epsilonproteobacteria* (Engel et al., 2003).

Gammaproteobacteria was found to represent ~43.59% of the community (Table 10, Table 11). Members of this class are known filamentous sulfur-oxidizers including *Thiothrix unzii,* which was used to inoculate CDC 1 and is consistent with previous investigations that found *Epsilonproteobacteria* and *Gammaproteobacteria* dominate the sulfur oxidizing communities in the stream biomats at LKC (Engel et al., 2003). In the Engel (2004) study, however, microorganisms representing the *Gammaproteobacteria* class were found to represent merely 12.2% of the total community (Engel et al., 2004.

The next most abundant class found in this sample were representatives of the *Deltaproteobacteria* class (Table 10). *Deltaproteobacteria* represent only ~0.43% of the counts. Members of *Deltaproteobacteria* are known sulfur-reducers such as *Desulfovibrio, Desulfotalea, Desulfonema, Desulfosarcina, Desulfobacter, Desulforomonas, and Geobacter* (Sievert et al., 2007). Previous phylogenetic analysis of LKC biomat communities found that *Deltaproteobacteria* represent 0.8% of the community population (Engel et al., 2003).

Most of the class level phylogenetic analysis performed in this study aligns well with previous studies. It should be noted here that previous studies found a significant abundance of *Betaproteobacteria* (11.7%), *Acidobacterium* (5.6%), and *Bacteroides/Chlorobi* (1.7%) within the biomats communities within LKC (Engel et al. 2003). The phylogenetic analysis performed for the study herein found

Betaproteobacteria (0.22%) and *Bacteroides/Chlorobi* (0.3)% within the biomats communities within LKC (Table 10).

Analysis of this phylogenetic data reveals two dominant genera within the inoculant that represent ~97.42% of the total counts (Table 12, Table 13). The most abundant genus is *Sulfurovum* which represents ~53.84% of the total counts. *Sulfurovum* is an *Epsilonproteobacteria* (Sievert et al., 2007). It is known to be a mesophilic microaerobe that uses sulfur species as electron donors with nitrate or oxygen as electron acceptors (Huber et al., 2007).

Thiothrix was found to represent another ~43.57% of the counts (Table 12, Table 13). The dominance of *Thiothrix* within the biomats sample does conform with previous studies of LKC (Engel et al., 2004). As discussed earlier, members of this genus are generally known as filamentous, sulfur-oxidizing microorganisms and a representative species (*Thiothrix unzii*) was used to inoculate CDC 1 for the biofilm experiments.

Sulfurospirillum is the next most abundant genus representing ~0.41% of the microbial community (Table 12). *Sulfurospirillum* is known to be a sulfur-reducing member of the *Epsilonproteobacteria* (Sievert et al., 2007). *Sulfurospirillum* is microaerophilic to anaerobic and so will dominate over sulfur-oxidizers in a mixed culture under anaerobic conditions (Sievert et al., 2007).

4.3 Effects of Mineralogy on Colonization and Dissolution

Mineral dissolution/colonization by microbial communities is typically the result of (1) energy demand, (2) use of the mineral as a terminal electron acceptor, (3) trace

element scavenging (Fe, K, P), (4) or in this case neutralization of generated acidity. Other, more specific reasons for dissolution/colonization of minerals include (1) phosphate mineral dissolution for construction of DNA, RNA, ADP, ATP, phospholipids, and polyphosphates (Jansson, 1987), and (2) sulfide and ferromagnesian silicate dissolution for enzyme cofactors (Banfield et al., 1999).

Observed high biomass accumulations on carbonates (Table 9) is likely due to an affinity of acid-generating neutrophiles for acid-buffering surfaces. The acid-buffering capacity of limestone and dolostone allows for the greatest microbial accumulation with a purely sulfur-oxidizing community (*Thiothrix unzii*) and a mixed culture from a sulfuric acid cave (CDC 2, 3, & 4). This is supported by the lack of dissolution features in abiotic reactors at both pH 6.9 and pH 8.3 when compared to corrosion features observed on the carbonate mineral coupon surfaces that were colonized by microbial communities (Figures 14 through 27). These results also show that biofilm accumulation variations were independent of bulk media pH.

The exception is the calcite coupons. Regardless of conditions, calcite coupons consistently accumulate very little biomass despite its ability to provide buffering capacity. This may be a result of the relative purity of Iceland spar calcite used in this experiment: the lack of internal micronutrients in the bulk media may not provide a critical component in this nutrient limited system. This hypothesis is supported by microbial accumulation studies on silicates that reveal that phosphorus- and iron-bearing silicate glasses were preferentially colonized and weathered, while glasses without these

elements were typically barren of colonizing microorganisms in subsurface microcosms (Rogers and Bennett, 2004).

The conclusions of Rogers and Bennett (2004) also may help explain the lack of microbial accumulation on the silicate mineral substrata vs. the high accumulation on basalt. In contrast to quartz, dissolution of feldspars generates soluble aluminum species which can be toxic to microbes (Konhauser 2007). The silicate mineral species used in these experiments fail to provide sufficient acid buffering capacity that is required by the neutrophilic microbes from LKC (Table 10, 11, 12, & 13) (Engel et al., 2004), while also releasing aluminum.

The basalt substratum appeared to accumulate mainly filamentous microbial populations in the mixed culture experiments (Figure 12D). Most of the filaments are of a morphology that is similar to that of the *Thiothrix unzii* filaments that were used in CDC 1 (Figures 11D, 16A). If these filamentous microorganisms are closely related to either *Thiothrix unzii* or *Sulfurovum,* as is likely, the implications are significant. Both *Thiothrix spp.* and *Sulfurovum* are known to be sulfur-oxidizing genera commonly associated with deep-sea hydrothermal vents at mid-ocean ridge spreading centers. This implies that the dominance of *Thiothrix spp.* on basalt is likely due to its superior ability to extract, and so take advantage of, mineral-bound nutrients in basalt. The laboratory bulk media is phosphate-limited to these microorganisms and their dominance is possibly due to the abundance of phosphate inclusions in the basalt sample (Bennett et al., 2001) combined with the adaptive ability of these microorganisms to efficiently extract nutrients from basalt.

4.3.1 LKC CDC FIELD REACTOR INCONSISTENCIES

Calculated $\Omega_{calcite}$ was 0.98 at 193 m in LKC and 1.08 within the LKC CDC reactor (Table 5). The slight increase in $[Ca^{2+}]$ measured in downstream waters may be due to dissolution of streambed calcite due to oxidation of sulfide, which corresponds with either the measured small increase in sulfate or possibly due to dissolution of gypsum that is prevalent within the cave as breakdown. Despite conditions of near equilibrium or slight supersaturation with respect to calcite, SEM images of the calcite mineral chips revealed corrosion features similar to those observed in laboratory reactors (Figure 25). This is consistent with results presented by Steinhauer et al., (2010). However, SEM images of the Madison Limestone and Madison Dolostone chips did not reveal the aggressive corrosion features observed in laboratory experiments (Figure 26, Figure 27), which is not consistent with those found in the Steinhauer et al. (2010) study.

Steinhauer et al. (2010) documented aggressive corrosion on both limestone and calcite chips, however there are some differences in experimental variables must be noted. Two separate studies were conducted by Steinhauer et al. (2010): one set of chips was left in the cave stream for several months and were placed in direct contact with the stream biomat, while the other experiment required rafting of filaments and fresh colonization. The experiment in direct contact showed much more aggressive mineral corrosion and much greater biofilm accumulation than the experiment where the microbes were required to raft and colonize the surface (Steinhauer et al. 2010).

In contrast, the LKC CDC reactor was inoculated with LKC microbial mat material and fed filtered cave stream water. Furthermore, the residence time of this water

was ~7 minutes within the LKC CDC. This short residence time likely does not allow enough time for the microbial populations to impact the pH of the solution, and while it was clear from the Steinhauer et al. (2010) experiments that "limestone rapidly dissolves where there is microbial colonization," (Steinhauer et al., 2010 pp. 733-734) neither Madison Limestone nor Madison Dolostone were subject to the corrosion observed in the laboratory CDC experiments described herein. This is likely due to both mineralogy and residence time.

Observations of biofilm accumulation on the carbonate minerals within LKC CDC reactor is consistent with laboratory experiments, but the apportionment of biofilm between the carbonate substrates in the field is much different than that of the laboratory experiments. The mean dry mass accumulations of the mixed culture CDC lab experiments on limestone and dolostone are 7.8 and 7.9 times higher than that of calcite, while the LKC CDC reactor had dry mass accumulation on limestone and dolostone of 2.1 and 2.3 times higher than that of calcite (Table 9). The much thinner biofilm on calcite allows diffusion of Ca^{2+} ions through the biofilm while still exposing the mineral surface to acidity generated by microorganisms adhered to that surface. The lower concentration of reduced sulfur within LKC would immediately be oxidized by microorganisms in direct contact with the bulk media. Therefore, a thinner biofilm would have metabolically-active sulfur-oxidizers in direct contact with the mineral surface resulting in more corrosive morphologies on the carbonate mineral surfaces. The thicker biofilms (relative to LKC CDC calcite biofilm) on Madison Limestone and Madison Dolostone in the cave environment may limit this diffusion of Ca^{2+} from the

microenvironment while limiting the direct contact of sulfur oxidizing microbes with the carbonate mineral surface (Luttge et al. 2005). Biofilm coverage will also reduce the reactive mineral surface area exposed bulk media.

The combination of these factors would cause dissolution to be less apparent on limestone and dolostone within LKC CDC until sufficient time has passed as to allow microbial sulfur metabolism to gain an advantage over these limitations. If this experiment had run for a longer time (say 3 weeks, it is hypothesized that dissolution features would be as apparent as those found in the laboratory experiments. This exemplifies the limitation of not being able to test the chemistry of the sub-biofilm microenvironment.

5 Conclusions

I examined the relationship between microbial sulfur metabolism and limestone dissolution in order to better understand and quantify the impact of said microbial metabolism on the rate of limestone dissolution within a sulfuric acid cave setting. The results of laboratory chemostat reactor experiments demonstrated that a chamber inoculated with a biomat community dominated by neutrophilic sulfur-oxidizing microorganisms, namely *Thiothrix* and *Sulfurovum*, can increase limestone dissolution rate by up to 3.3 times (Figure 6).

Microorganisms in these communities will convert an external sulfur source, in this case S_2O_3, into internal S^o and utilize this internal electron donor during times of external limitations. This ability led to instability in the biotic chamber pH that was highly dependant on the concentration of thiosulfate and O_2 supplied (Figure 6). The pH response to O_2 limitations is contradictory to the findings by Steinhauer et al., 2010 which found that changes in O_2 limitations had very little (if any) affect on pH of a similar biotic chemostat (Steinhauer et al., 2010). The airtight construction of the laboratory chemostat chambers described herein allowed complete consumption of oxygen when the air supply was closed, making the impact of O_2 limitations measureable.

These experiments also demonstrated that under oxygen limitations the microbial community biofilms composed mainly of SOB (*Thiothrix* and *Sulfurovum*) can actually limit diffusion of ions away from the mineral surface and slow limestone dissolution to

less than abiotic rates (Table 7). This effect may be exacerbated by the presence of sulfur reducing bacteria within the ecosystem. Although sulfur reducing bacteria were found to represent less than 3% of the initial inoculant community, it is possible that the initial anaerobic conditions allowed them to dominate for the periods without oxygenation of media.

Experiments investigating the dry mass accumulation on a variety of minerals under a variety of conditions confirmed that microbial communities composed mainly of sulfur-oxidizing, neutrophilic microorganisms accumulate substantially more biomass on Madison Limestone and Madison Dolostone than on silicate minerals when given an equal opportunity to colonize (Table 9). This is most probably due to the buffering capacity that is supplied by the carbonate minerals, but not by the silicates. Iceland spar calcite does not accumulate adequate biomass to also support this hypothesis. This is likely due to the lack of micronutrients within Iceland spar calcite compared to Madison Limestone and Madison Dolostone. In the nutrient limited system that I created, specific microbes seek out minerals that can fulfill nutrient requirements which cannot be fulfilled by the liquid medium (namely P and N).

This also explains the relatively high accumulation weights on basalt coupons in all reactor experiments when compared to the other silicates (Table 9). Images of silicates in LKC CDC reveal that the biomass accumulating on basalt is uniquely filamentous (Figure 12). After reviewing these images of *Thiothrix unzii* and analyzing the phylogenetic data it seems likely that a majority of the filamentous biofilm is composed of *Thiothrix spp.* and *Sulfurovum spp.* (Figure 11, Figure 16, and Table 13).

This relationship is likely due to the ability of these microorganisms to more effectively extract micronutrients from the basalt (namely P).

This same series of CDC reactor experiments also confirmed that microbial biofilms of sulfur oxidizing bacteria aggressively corrode carbonate minerals by physically separating the bulk media from the sub-biofilm environment. Abiotic reactors run at both pH of 8.3 and pH 6.6 showed no evidence of carbonate corrosion on a variety of carbonates (Figure 13, Figure 14). A reactor inoculated with a pure culture of *Thiothrix unzii* showed aggressive corrosion of all carbonate substrates within the reactor (Figure 15, Figure 16, and Figure 17). Reactors inoculated with a mixed culture composed mainly of sulfur oxidizers of the genera *Thiothrix* and *Sulfurovum* showed aggressive corrosion of all carbonate substrates at pHs of 6.6 and 8.3 within calcite equilibrated media (Figure 18, Figure 19, Figure 20, Figure 21, Figure 22, Figure 23, and Figure 24). Calcite shows the same type of "spiky" morphology in all of these reactors. LKC CDC shows the same aggressive corrosion on calcite, but very little on limestone or dolostone in reactor media with $\Omega_{calcite}$ of 1.08 (Figure 25, Figure 26, and Figure 27). However this experiment was only conducted for one week compared to three weeks for all other reactors. I believe there to be limited sulfur metabolism for the initial period of colonization on Limestone and Dolostone. During this lag in metabolism, the accumulating biomass also acts to limit diffusion of ions into solution. This would also hinder carbonate dissolution.

Future endeavors into the impact of microorganisms on mineral dissolution may need to consider the impact of nutrient limitations in media, and micronutrients within solid substrate on microbial metabolism and population accumulation.

TABLES.

Element		Oligoclase (Albite)	Plagioclase (Kspar)	Quartz	Basalt
SiO2	(%)	62.97	59.8	99.78	51
Al2O3	(%)	22.72	20.87	0.08	13.65
Fe2O3	(%)	1.3	1.07	0.02	14.12
MgO	(%)	0.03	0.08	<0.01	4.54
CaO	(%)	4.51	2.37	0.01	8.93
Na2O	(%)	8.16	6.69	<0.01	2.67
K2O	(%)	0.6	7.37	0.03	1.07
TiO2	(%)	<0.01	<0.01	<0.01	3.11
P	(ppm)	130	<50	90	3010
Ba	(ppm)	51	438	<2	505
Zr	(ppm)	1	<2	<2	175
Cu	(ppm)	11	6	8	24
Pb	(ppm)	46	28	<5	6.2
Zn	(ppm)	6	3	2	126
Ni	(ppm)	19	2	14	85
Mn	(ppm)	106	57	73	896
Sr	(ppm)	230	399	5	314

Table 1. Whole rock and trace metal element analysis of select minerals used in CDC reactor experiments. Adapted from Bennett et al., 2001.

Lower Kane Cave Major Constituent Water Chemistry Data (2010) (UNITS mM)													
D (m)	^0C	pH	DO (ppm)	Si	Ca	Mg	Na	K	SO_4^{2-}	HCO_3^-	Cl	NO_3^{2-}	$\Omega_{calcite}$
112	22	7.34	0.37	0.19	1.81	1.15	0.31	0.05	1.17	3.48	0.22	0.00	0.97
118	22	7.26	1.39	0.19	1.78	1.15	0.34	0.05	1.17	3.52	0.23	0.13	0.80
191	22.1	7.04	0.78	0.21	1.75	1.09	0.42	0.06	1.17	3.52	0.22	0.00	0.48
193	22.1	7.14		0.19	1.66	1.05	0.30	0.05	1.17	3.56	0.21	0.06	0.58
196	22.1	7.15	1.28	0.19	1.72	1.11	0.31	0.05	1.19	3.56	0.20	0.05	0.61
248	21.8	6.99	1.41	0.19	1.81	1.18	0.41	0.05	1.12	3.32	0.18	0.00	0.41
249	21.8	6.92	1.42	0.19	1.74	1.10	0.30	0.05	1.17	3.32	0.21	0.06	0.58

Table 2. Lower Kane Cave Major Constituent Water Chemistry Data (2010)

Lower Kane Cave Minor Constituent Water Chemistry Data (2010) (UNITS µM)											
D (m)	pH	Sr	Fe_{Tot}	F	Al	Ba	Mn	Mo	Ni	V	Zn
112	7.34	7.88	0.17	33.60	0.01	0.30	0.02	0.05	0.04	0.04	0.11
118	7.26	7.67	0.28	32.26	0.02	0.29	0.02	0.06	0.04	0.04	0.10
191	7.04	7.28	0.16	30.47	0.09	0.29	0.03	0.06	0.04	0.04	0.09
193	7.14	7.10	0.30	36.17	0.34	0.28	0.03	0.06	0.03	0.04	0.04
196	7.15	7.47	0.15	33.48	0.02	0.29	0.02	0.06	0.03	0.04	0.11
248	6.99	7.80	0.17	37.09	0.05	0.30	0.02	0.06	0.04	0.05	0.08
249	6.92	7.42	0.16	33.49	0.22	0.29	0.03	0.07	0.03	0.05	0.09

Table 3. Lower Kane Cave Minor Constituent Water Chemistry Data (2010)

Lower Kane Cave Major Constituent Water Chemistry Data (2011) (UNITS mM)													
D (m)	^0C	pH	DO (ppm)	Si	Ca	Mg	Na	K	SO_4^{2-}	HCO_3^-	Cl	NO_3^{2-}	$\Omega_{calcite}$
118	21.7	7.3	0.23	0.18	1.62	1.01	0.27	0.04	1.19	3.24	0.18	0.01	1.26
191	21.9	7.28	0.27	0.18	1.65	1.06	0.27	0.04	1.18	3.16	0.18	0.04	1.19
193	21.9	7.28	0.26	0.18	1.34	0.86	0.22	0.03	1.14	3.20	0.18	0.01	0.98
196	21.9	7.31	0.34	0.18	1.61	1.02	0.26	0.04	1.16	3.20	0.19	0.03	1.26
199	21.9	7.3	0.46	0.18	1.50	0.97	0.25	0.04	1.16	3.20	0.18	0.03	1.15
202	21.9	7.32	1.07	0.17	1.77	1.11	0.28	0.04	1.19	3.16	0.19	0.02	1.41
205	21.9	7.33	1.50	0.18	1.61	1.00	0.25	0.04	1.28	3.24	0.18	0.01	1.34
248	21.6	7.4	0.55	0.18	1.71	1.04	0.27	0.04	1.15	3.16	0.31	0.00	1.63
249	21.9	7.42		0.17	1.44	0.94	0.24	0.04	1.17	3.16	0.17	0.01	1.44
LKC CDC	22	7.39		0.18	1.55	0.98	0.25	0.04	1.16	3.20	0.18	0.00	1.08

Table 4. Lower Kane Cave Major Constituent Water Chemistry Data (2011)

Lower Kane Cave Minor Constituent Water Chemistry Data (2011) (UNITS µM)											
D (m)	pH	Sr	Fe_{Tot}	F	Al	Ba	Mn	Mo	Ni	V	Zn
118	7.3	7.63	0.05	55.10	0.02	0.30	0.01	0.05	0.03	0.04	0.00
191	7.28	7.75	0.03	64.04	0.01	0.31	0.01	0.06	0.03	0.04	0.02
193	7.28	6.22	0.26	47.46	0.04	0.25	0.01	0.06	0.02	0.04	0.07
196	7.31	7.48	0.04	63.38	0.01	0.31	0.01	0.06	0.03	0.04	0.01
199	7.3	6.98	0.04	52.82	0.02	0.28	0.01	0.06	0.02	0.04	0.01
202	7.32	8.18	0.10	54.87	0.06	0.34	0.01	0.06	0.03	0.05	0.01
205	7.33	7.15	0.06	52.76	0.03	0.29	0.01	0.06	0.02	0.04	0.01
248	7.4	7.99	0.02	49.90	0.05	0.33	0.01	0.07	0.03	0.05	0.03
249	7.42	6.75	0.02	50.53	0.04	0.27	0.01	0.06	0.02	0.04	0.01
LKC CDC	7.39	7.10	0.06	52.65	0.03	0.28	0.01	0.06	0.02	0.04	0.02

Table 5. Lower Kane Cave Minor Constituent Water Chemistry Data (2011)

Time (Hours)	Flow Rate (ml/min)	Geometric Surface Area (cm^2)	Hardness as Ca^{2+} (mMol/L)	pH	DIC (mg/L)	Abiotic Dissolution Rate (mol cm^{-2} s^{-1})
44:50:00	1.21	180	1.79	8.2		8.85E-11
45:30:00	1.21	180	1.8	8.2		8.96E-11
46:20:00	1.21	180	1.7	8.2		7.84E-11
48:40:00	1.21	180	1.7	8.2		7.84E-11
73:30:00	1.21	180	1.6	8.2	12.9222	6.72E-11
90:30:00	1.21	180	1.55	8.2	12.4434	6.16E-11
209:50:00	1.21	180	1.6	8.11		6.72E-11
210:40:00	1.21	180	1.6	8.11		6.72E-11
213:45:00	1.21	180	1.6	8.08		6.72E-11
215:00:00	1.21	180	1.6	8.08	13.5988	6.72E-11
215:15:00	1.21	180	1.8	8.07	13.5435	8.96E-11
236:30:00	1.21	180	1.79	8.07	14.1174	8.85E-11
237:00:00	1.21	180	1.74	8.06	13.5623	8.29E-11
237:15:00	1.21	180	1.75	8.05		8.40E-11
261:25:00	1.21	180	1.8	8.04		8.96E-11
261:40:00	1.21	180	1.825	8.04		9.24E-11
262:00:00	1.21	180	1.7	8.04	13.2124	7.84E-11
262:20:00	1.21	180	1.65	8.03		7.28E-11
335:30:00	1.21	180	1.6	7.8	11.3858	6.72E-11
336:00:00	1.21	180	1.6	7.8	10.4758	6.72E-11
358:30:00	1.21	180	1.55	7.8	6.2244	6.16E-11
359:30:00	1.21	180	1.65	7.8		7.28E-11
380:50:00	1.21	180	1.55	7.8	5.1697	6.16E-11
405:15:00	1.21	180	1.5	7.8		5.60E-11
428:30:00	1.21	180	1.6	7.82		6.72E-11

Table 6. Measured abiotic dissolution rate and select changes in geochemistry within the abiotic chemostat chamber.

Time (Hours)	Flow Rate (ml/min)	Geometric Surface Area (cm^2)	Hardness as Ca^{2+} (mMol/L)	pH	DIC (mg/L)	Biotic Dissolution Rate (mol cm^{-2} s^{-1})	Biotic Rate Divided by Abiotic Rate
44:50:00	1.21	180	1.4	9.19		4.48E-11	0.51
45:30:00	1.21	180	1.3	9.194		3.36E-11	0.38
46:20:00	1.21	180	1.5	9.194		5.60E-11	0.71
48:40:00	1.21	180	1.45	9.173		5.04E-11	0.64
73:30:00	1.21	180	1.4	8.871	10.5061	4.48E-11	0.67
90:30:00	1.21	180	1.3	8.77	9.8759	3.36E-11	0.55
209:50:00	1.21	180	2.5	6.676		1.68E-10	2.50
210:40:00	1.21	180	2.4	6.674		1.57E-10	2.33
213:45:00	1.21	180	2.49	6.65		1.67E-10	2.48
215:00:00	1.21	180	2.49	6.65	4.2269	1.67E-10	2.48
215:15:00	1.21	180	2.1	6.644	5.7711	1.23E-10	1.38
236:30:00	1.21	180	2.4	6.608	4.4177	1.57E-10	1.77
237:00:00	1.21	180	2.8	6.603	5.8459	2.02E-10	2.43
237:15:00	1.21	180	2.45	6.602		1.62E-10	1.93
261:25:00	1.21	180	3.1	6.585		2.35E-10	2.63
261:40:00	1.21	180	2.95	6.595		2.18E-10	2.36
262:00:00	1.21	180	2.89	6.58	5.4751	2.12E-10	2.70
262:20:00	1.21	180	2.9	6.578		2.13E-10	2.92
335:30:00	1.21	180	3	5.573	1.651	2.24E-10	3.33
336:00:00	1.21	180	2.45	5.603	2.445	1.62E-10	2.42
358:30:00	1.21	180	2.5	5.85	1.7992	1.68E-10	2.73
359:30:00	1.21	180	2.8	5.85	1.8314	2.02E-10	2.77
380:50:00	1.21	180	2.4	6.1	1.6464	1.57E-10	2.55
405:15:00	1.21	180	2.65	6.3		1.85E-10	3.30
428:30:00	1.21	180	2.95	6.215		2.18E-10	3.25

Table 7. Measured biotic dissolution rate and select changes in geochemistry within the biotic chemostat chamber. Red shaded region emphasizes periods where biotic dissolution rate is slower than abiotic. Green shaded region emphasizes periods where biotic dissolution rate is faster than abiotic.

Measured Changes in Sulfur Species for Chemostats										
Hour	Input Media $S_2O_3^{2-}$ (mM)	Input Media SO_4^{2-} (mM)	Output $S_2O_3^{2-}$ (mM) Biotic	Output $S_2O_3^{2-}$ (mM) Abiotic	Biotic $S_2O_3^{2-}$ Loss (mM/hr)	Abiotic $S_2O_3^{2-}$ Loss (mM/hr)	Output SO_4^{2-} (mM) Biotic	Output SO_4^{2-} (mM) Abiotic	Biotic SO_4^{2-} Produced (mM/hr)	Abiotic SO_4^{2-} Produced (mM/hr)
73:30:00	10.98	1.35	10.88	10.98	0.01	0.00				
75:00:00	10.98	1.35	10.88	10.98	0.01	0.00				
209:50:00	10.98	1.35	5.36	7.37	0.68	0.44				
210:40:00	10.98	1.35	6.03	7.37	0.60	0.44				
213:45:00	10.98	1.35	8.04	7.37	0.35	0.44				
262:00:00	4.13	1.35	3.91	4.13	0.03	0.00				
262:30:00	4.13	1.35	3.91	4.13	0.03	0.00				
329:30:00	0.89	1.35	0.22	0.89	0.08	0.00				
334:15:00	0.89	1.35	0.22	0.89	0.08	0.00	3.89	1.56	0.31	0.03
334:55:00	0.89	1.35	0.22	0.89	0.08	0.00				
358:30:00	0.89	1.35	0.22	0.67	0.08	0.03	3.56	1.50	0.27	0.02
359:30:00	0.89	1.35	0.22	0.67	0.08	0.03				
380:15:00	0.89	1.35	0.22	0.67	0.08	0.03	3.46	1.51	0.25	0.02
380:30:00	0.89	1.35	0.22	0.67	0.08	0.03				
383:17:00	0.89	1.35	0.33	0.67	0.07	0.03				
383:30:00	0.89	1.35	0.33	0.67	0.07	0.03				
383:45:00	0.89	1.35	0.33	0.67	0.07	0.03				
405:15:00	0.89	1.35	0.56	0.67	0.04	0.03				
405:40:00	0.89	1.35	0.56	0.67	0.04	0.03	3.66	1.46	0.28	0.01
406:30:00	0.89	1.35	0.56	0.67	0.04	0.03				
407:30:00	0.89	1.35	0.56	0.67	0.04	0.03				

Table 8. Measured changes in sulfur species for chemostat experiments. Note that there is a greater loss rate (mM/hr) of thiosulfate at 0.89mM concentration than at 4.13mM.

Mineral	Dry Mass of Biofilm (mg/cm^2)						
	CDC 1 *T. unzii pH 6.6*	CDC 2 Mixed pH 6.6	CDC 3 Mixed pH 6.6	CDC 4 Mixed pH 8.3	LKC CDC	Mean of Mixed (LAB)	Mean Overall (LAB)
Calcite	2.3	2.0	2.4	2.7	2.3	2.4	2.3
Limestone	14.4	19.3	18.2	19.3	4.9	18.9	17.8
Dolostone	25.9	10.6	22.3	23.6	5.3	18.8	20.6
Kspar	1.18	0.63	0.55	0.24	*	0.5	*
Albite	1.18	1.50	0.87	1.11	*	1.2	*
Chert	0.39	0.47	0.39	0.63	*	0.5	*
Basalt	3.55	5.37	5.76	6.95	*	6.0	*
Quartz	1.50	2.92	1.50	2.13	*	2.2	*

Table 9. Dry Mass of biofilm (mg/cm^2) for CDC reactor experiments. Accumulation is consistently higher on Limestone and Dolostone substrates. (*) indicates no data for that cell.

Class Level 16S rRNA Data for 191m Biomat		
Class	Counts	Percent Abundance
Epsilonproteobacteria	3479	54.79%
Gammaproteobacteria	2768	43.59%
Deltaproteobacteria	27	0.43%
Bacteroidia	19	0.30%
Flavobacteria	15	0.24%
Betaproteobacteria	14	0.22%
Cytophagia	7	0.11%
Clostridia	5	0.08%
Alphaproteobacteria	4	0.06%
Anaerolineae	2	0.03%
Chloroflexi (class)	2	0.03%
Spirochaetes (class)	2	0.03%
Actinobacteria (class)	1	0.02%
Deinococci	1	0.02%
Flavobacteria::Cytophagia	1	0.02%
Lentisphaerae (class)	1	0.02%
Anaerolineae::Chloroflexi (class)	1	0.02%
Cyanobacteria (class)	1	0.02%
Total Counts	6350	100.00%

Table 10. Class level phylogenetic data for 191m biomat that was used to inoculate all mixed culture CDC reactors and LKC CDC.

Dominant Classes by 16S rRNA for 191m Biomat		
Class	Counts	Percent Abundance
Epsilonproteobacteria	3479	54.79%
Gammaproteobacteria	2768	43.59%
Total > 0.50%		98.38%

Table 11. Dominant Class level phylogenetic data for 191m biomat that was used to inoculate all mixed culture CDC reactors and LKC CDC.

Genus Level 16S rRNA Data for 191m Biomat		
Genus	Counts	Percent Abundance
Sulfurovum	3419	53.84%
Thiothrix	2767	43.57%
Sulfurospirillum	26	0.41%
Campylobacter	25	0.39%
Bacteroides	17	0.27%
Flavobacterium	12	0.19%
Geobacter	12	0.19%
Desulfocapsa	8	0.13%
Sterolibacterium	8	0.13%
Arcobacter	8	0.13%
Cytophaga	7	0.11%
Fusibacter	4	0.06%
Hydrogenophaga	2	0.03%
Levilinea	2	0.03%
Chloroflexus	2	0.03%
Spirochaeta	2	0.03%
Desulforhopalus::Desulfobacterium	2	0.03%
Thiobacillus	1	0.02%
Mitsuaria	1	0.02%
Fluviicola	1	0.02%
Byssovorax	1	0.02%
Leptothrix	1	0.02%
Denitratisoma	1	0.02%
Eubacterium	1	0.02%
Pseudorhodobacter	1	0.02%
Trichlorobacter	1	0.02%
Stenotrophomonas	1	0.02%
Desulfobacterium	1	0.02%
Paracoccus	1	0.02%
Methylocystis	1	0.02%
Marinithermus	1	0.02%
Desulfosarcina	1	0.02%
Alistipes	1	0.02%
Cytophaga (Lentisphaerae)	1	0.02%
Brachybacterium	1	0.02%
Desulfuromonas	1	0.02%
Xanthobacillum::Cytophaga	1	0.02%
Novosphingobium	1	0.02%
Levilinea::Chloroflexus	1	0.02%
Paludibacter	1	0.02%
Crocinitomix	1	0.02%
Synechococcus	1	0.02%
Xanthobacillum	1	0.02%
Sulfurovum::Arcobacter	1	0.02%
Total	6350	100.00%

Table 12. Genus level phylogenetic data for 191m biomat that was used to inoculate all mixed culture CDC reactors and LKC CDC. This figure starts on the previous page.

Dominant Classes by 16S rRNA for 191m Biomat		
Genus	Counts	Percent Abundance
Sulfurovum	3419	53.84%
Thiothrix	2767	43.57%
Total > 0.50%		97.42%

Table 13. Dominant Genus level phylogenetic data for 191m biomat that was used to inoculate all mixed culture CDC reactors and LKC CDC.

Sample	Phylogenetic Level	No. Counts	Number of Phylotypes Observed	Shannon-Wiener (H')	Evenness (E)	Simpson's Index (D)
LKC 191m	Class	6350	18	0.79	0.27	0.49
LKC 191m	Genus	6350	44	0.87	0.23	0.48
190m (Engel 2004)		127	10	1.36	0.39	0.65
195m (Engel 2004)		117	10	1.24	0.54	0.38

Table 14. Bacterial coverage and ecological indices for LKC 191m biomat compared to indices from Engel 2004 dissertation.

FIGURES

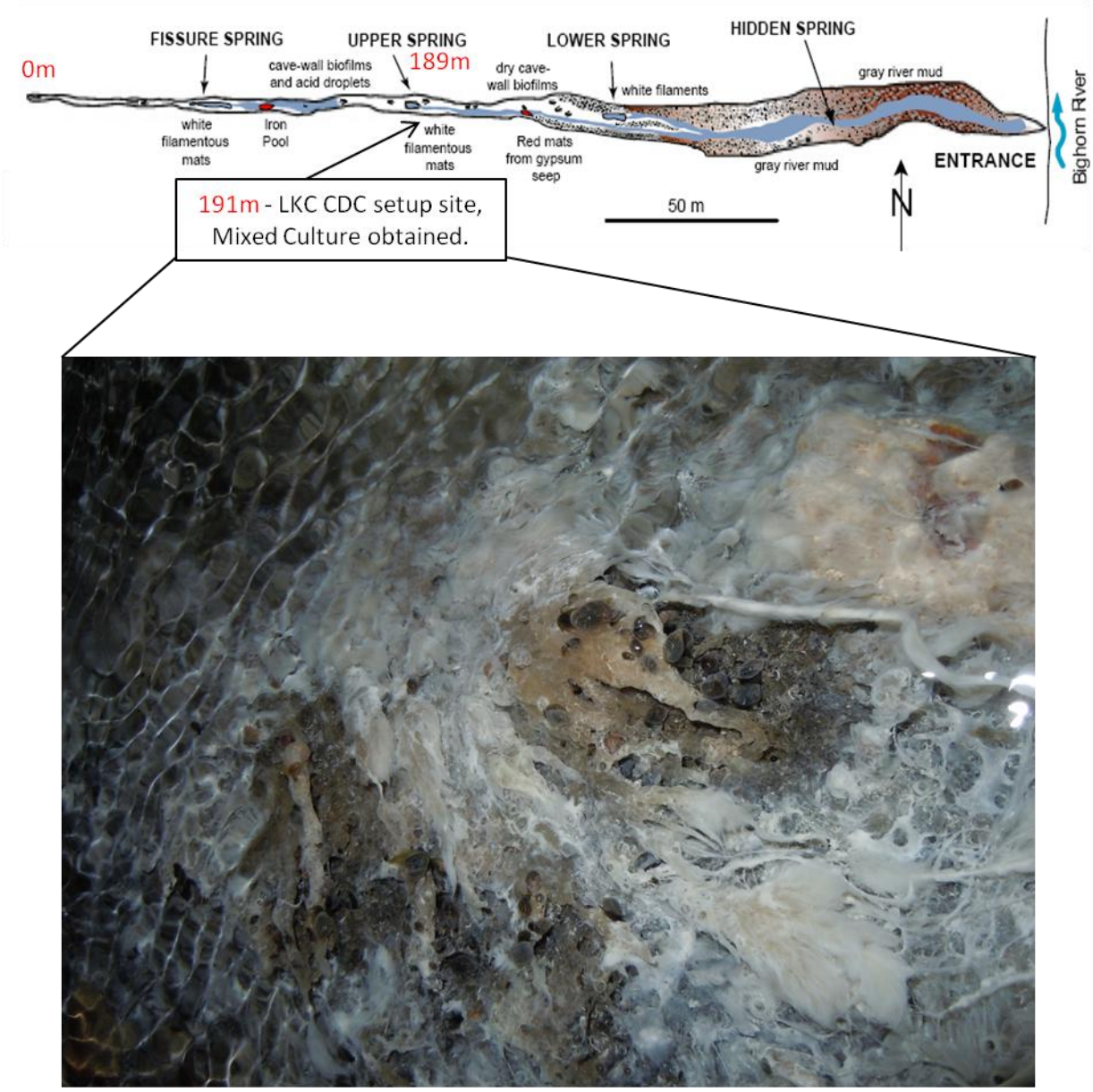

Figure1. Plan view of Lower Kane Cave with LKC CDC site with mixed culture sampling sight emphasized. Modified from Egemeier (1981). Snales in the image vary in size from 0.2 to 0.5 cm.

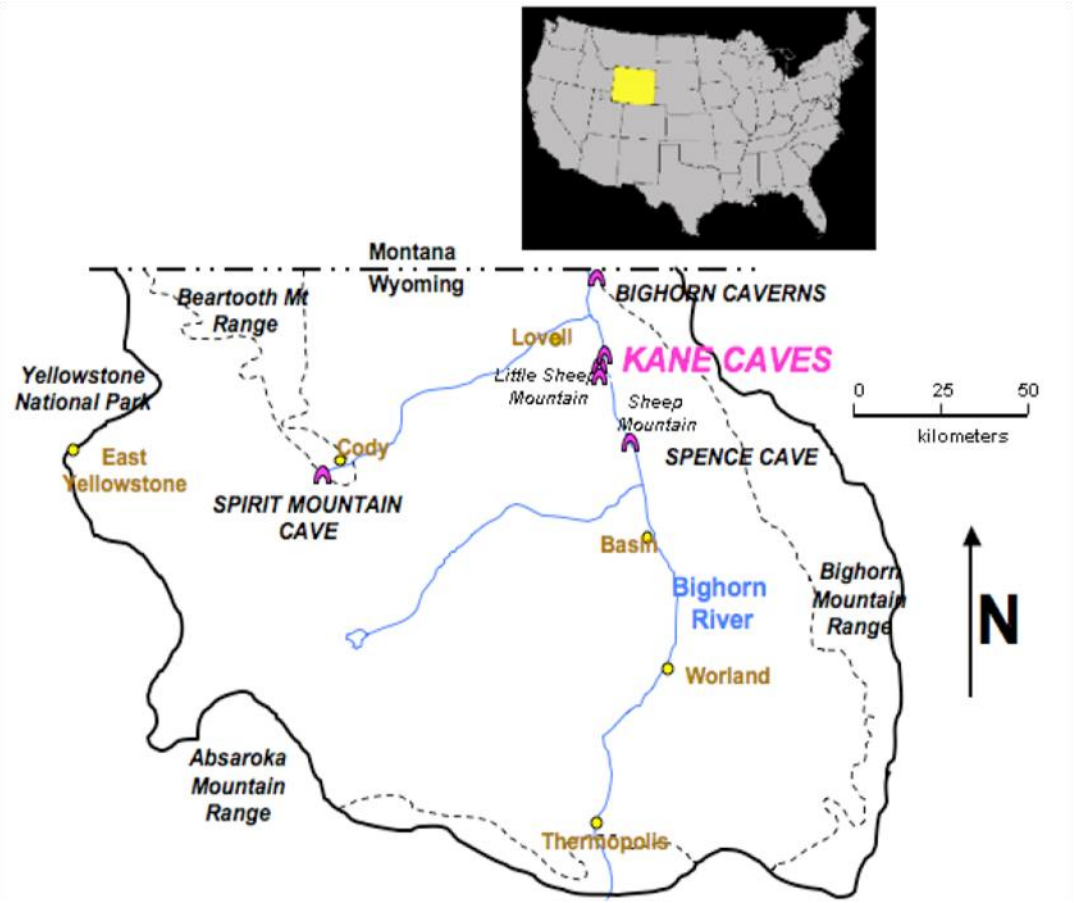

Figure 2. Map of Bighorn Basin, WY. With Kane Caves located in the Little Sheep Mountain anticline near Lovell, WY. Obtained from Steinhauer 2008 Thesis.

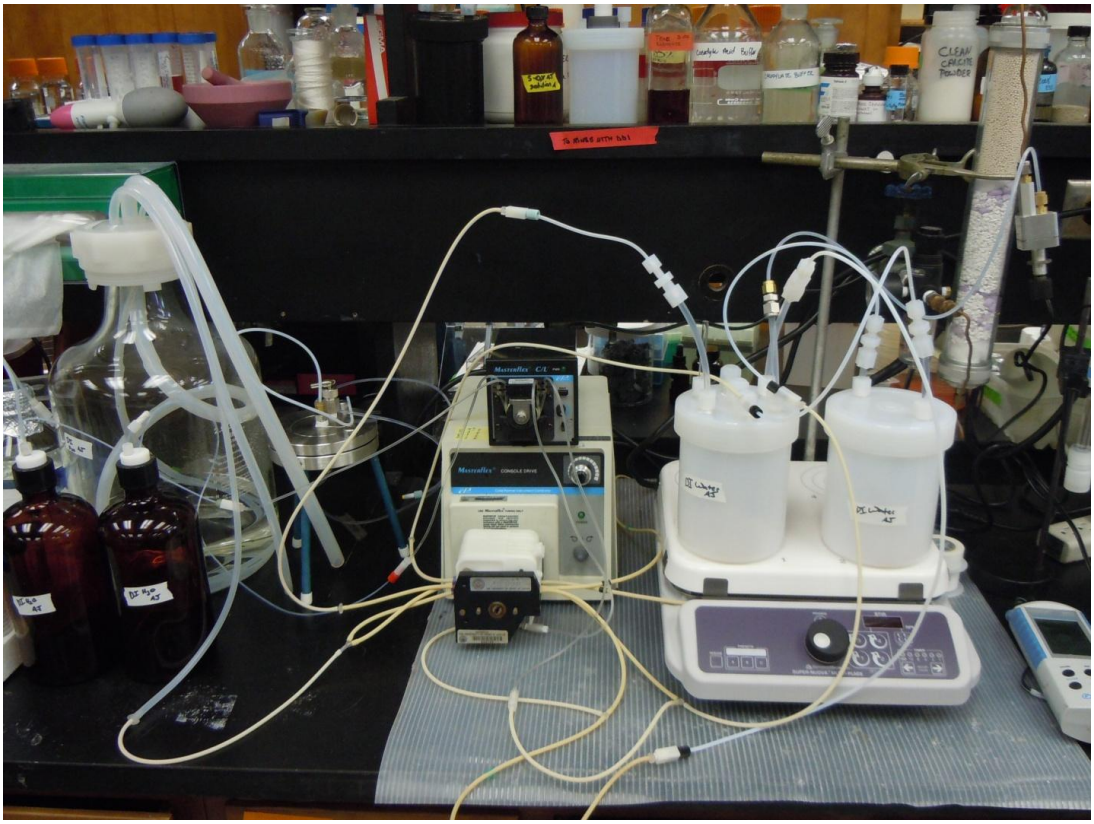

Figure 3. Laboratory chemostat chambers for determining rate of limestone dissolution. 2-1L teflon reactors. Abiotic (Left), Biotic (right). Bulk Media in 9.5L carboy.

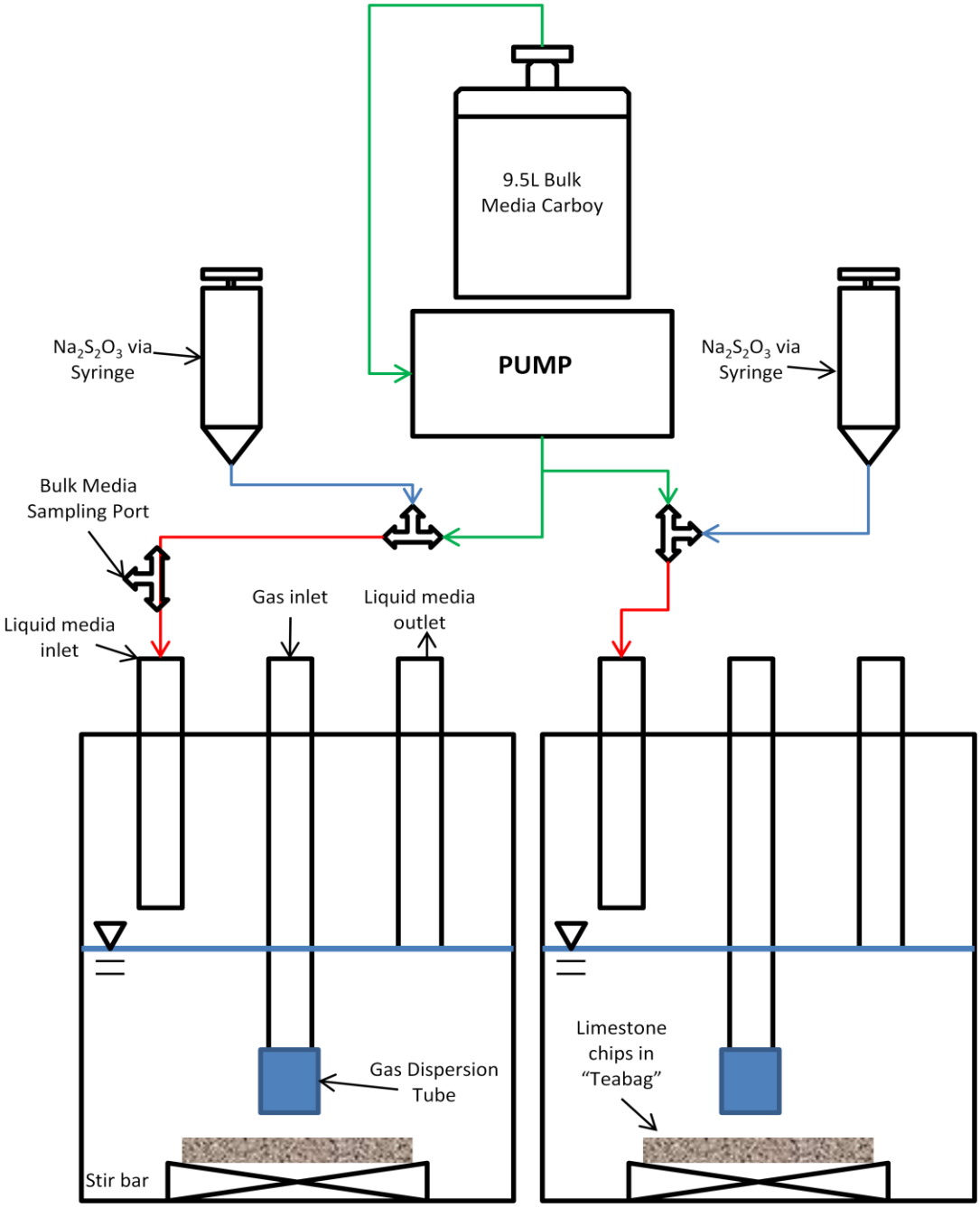

Figure 4. Schematic of laboratory chemostat chambers for limestone dissolution rate experiments. Biotic chamber (left) and abiotic chamber (right) are identical. Green lines indicate bulk media tubing, blue lines indicate $Na_2S_2O_3$ tubing, and red lines indicate tubing carrying chamber input solution. Unlabeled ports on the right reactor are used for the same purpose as in the left reactor.

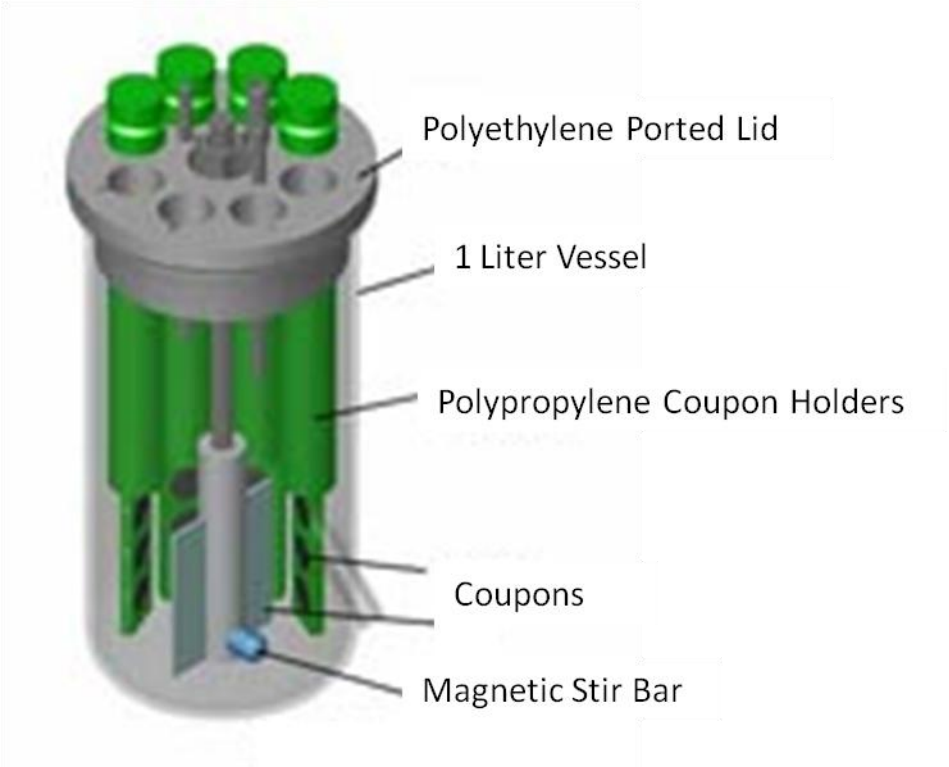

Figure 5. CDC biofilm reactor schematic. Reactor maintains a constant volume of 400 ml at a flow rate of 1.2 ml/min. This reactor was used for biofilm experiments CDC 1, 2, 3, 4, & LKC CDC. From http://www.biofilms.biz/biofilm-reactors.

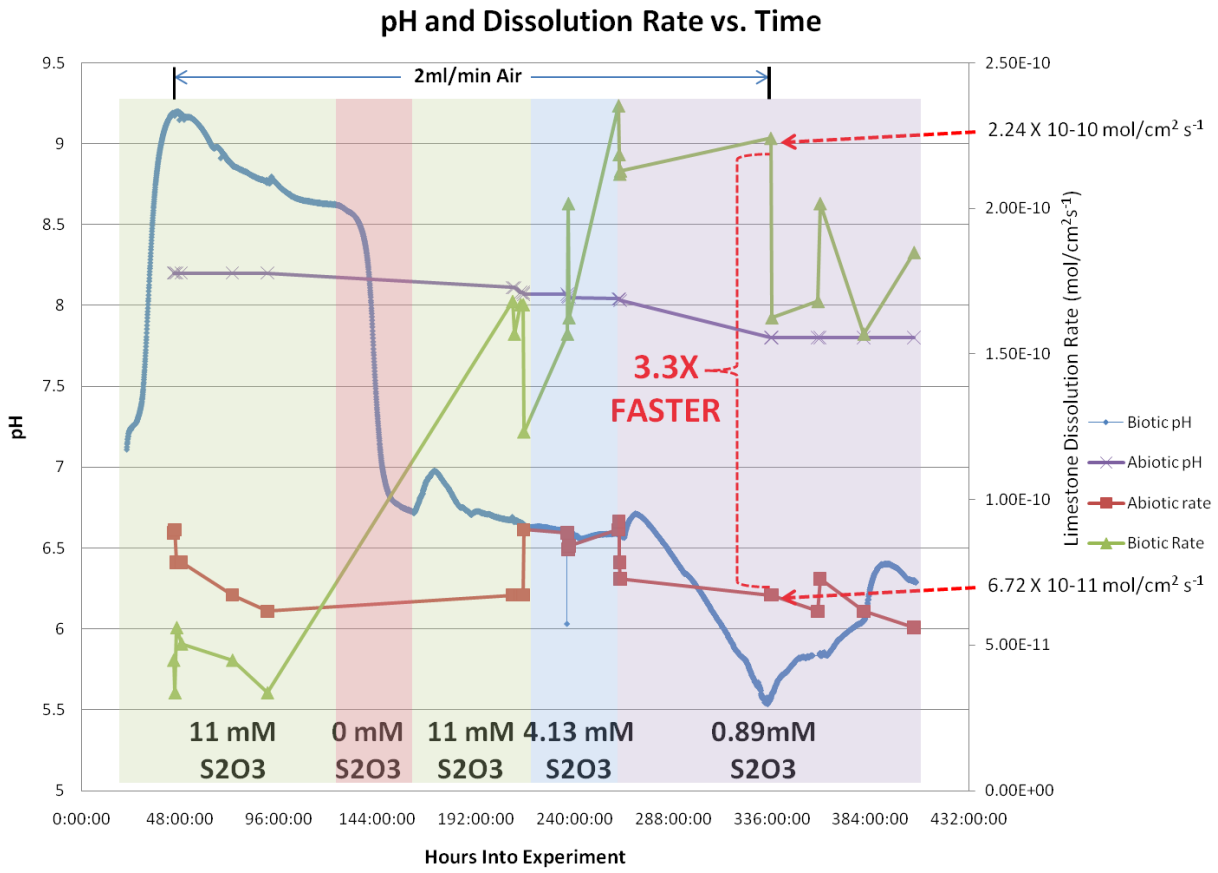

Figure 6. Plot of pH and Limestone dissolution rate ($mol \cdot cm^{-2} \cdot s^{-1}$ vs. time (hours) for both biotic and abiotic chemostat chambers. Colored/shaded regions denote thiosulfate concentrations for a particular span of time. Greatest disparity in dissolution rate between biotic and abiotic chambers is highlighted. Note the effect of Air flow and variable $S_2O_3^{2-}$ concentration on biotic pH.

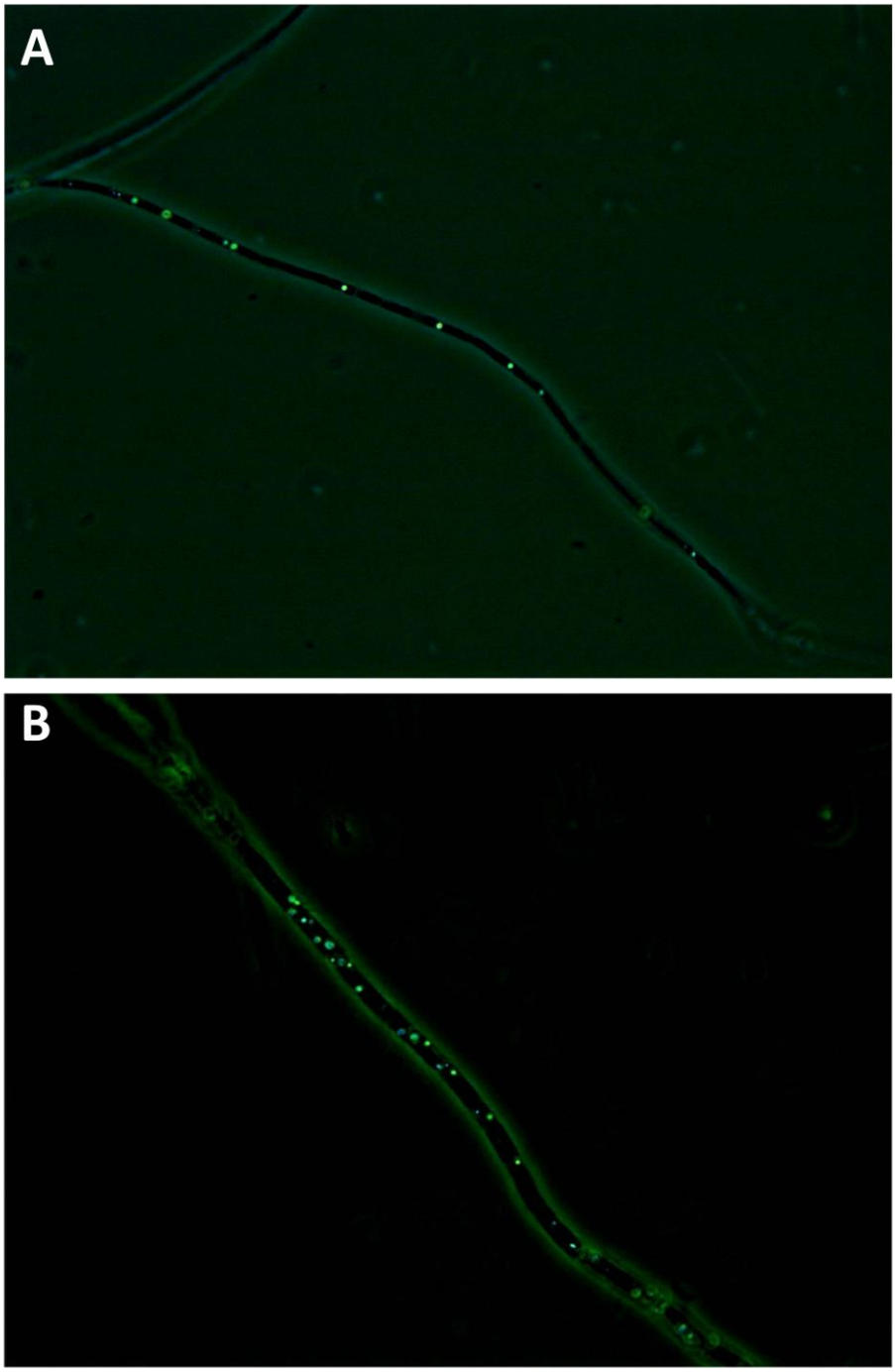

Figure 7. Light microscope images of microbial filaments obtained from within the biotic reactor after 45 hours in the reactor. (A) shows a thin filament with glowing internally stored sulfur. (B) shows thicker filament with glowing internally stored sulfur. Image was captured under 100X magnification.

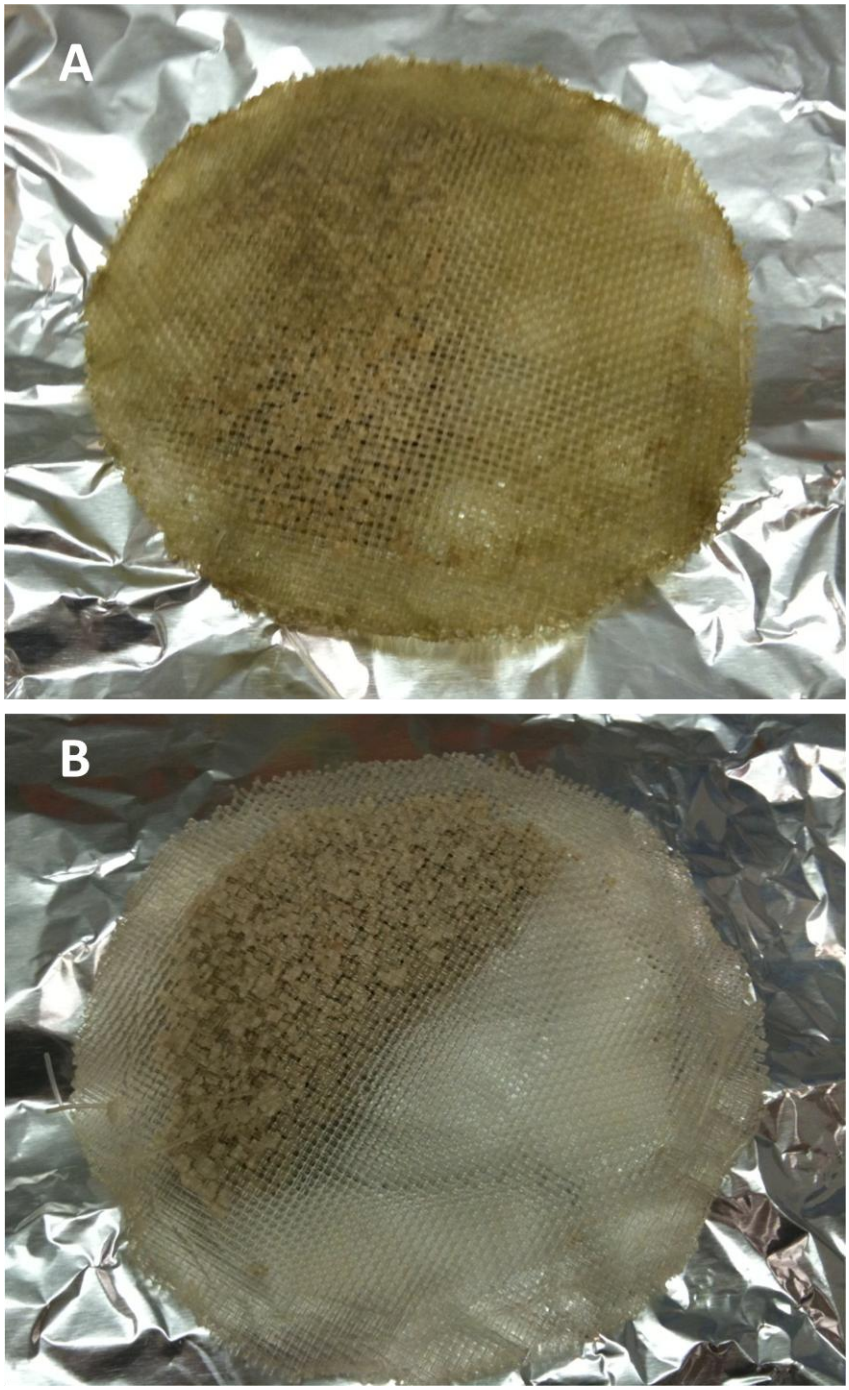

Figure 8. Mesh “Teabags” after removal from (A) biotic and (B) abiotic chemostat. Teabag A has evident biofilm accumulation. Teabags are ~8.5 cm in diameter.

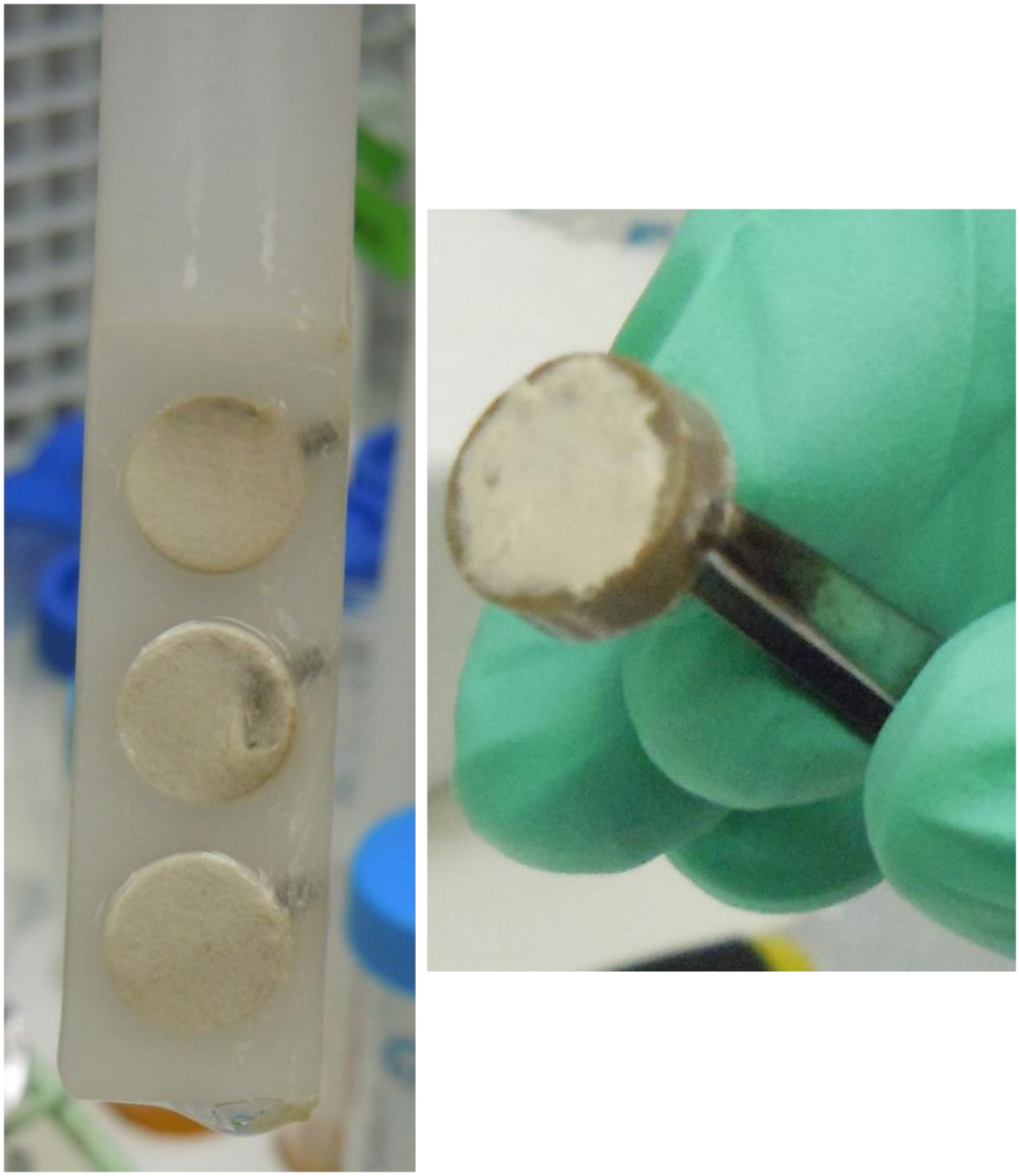

Figure 9. Madison Limestone coupons after three weeks in CDC 1. This image shows filamentous *Thiothrix unzii* (white) growing on the coupon surface. Mineral coupons are ½ inch (12.7 mm) in diameter.

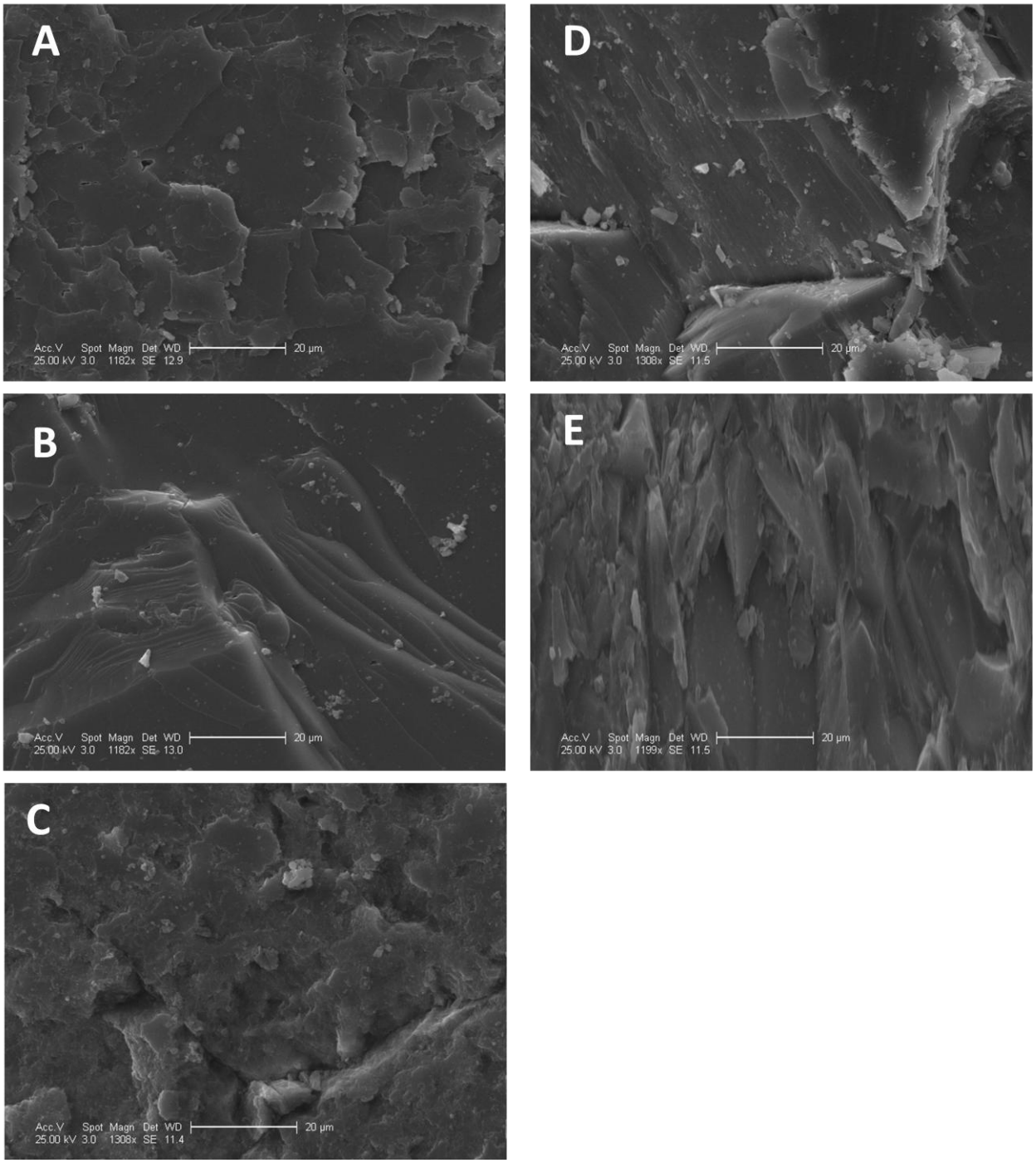

Figure 10. SEM images of silicate coupons retrieved from Abiotic CDC reactor performed at pH = 6.6 after 3 weeks in reactor. A is Kspar, B is Albite, C is Chert, D is Basalt, E is Quartz. Scale bar is 20 μm.

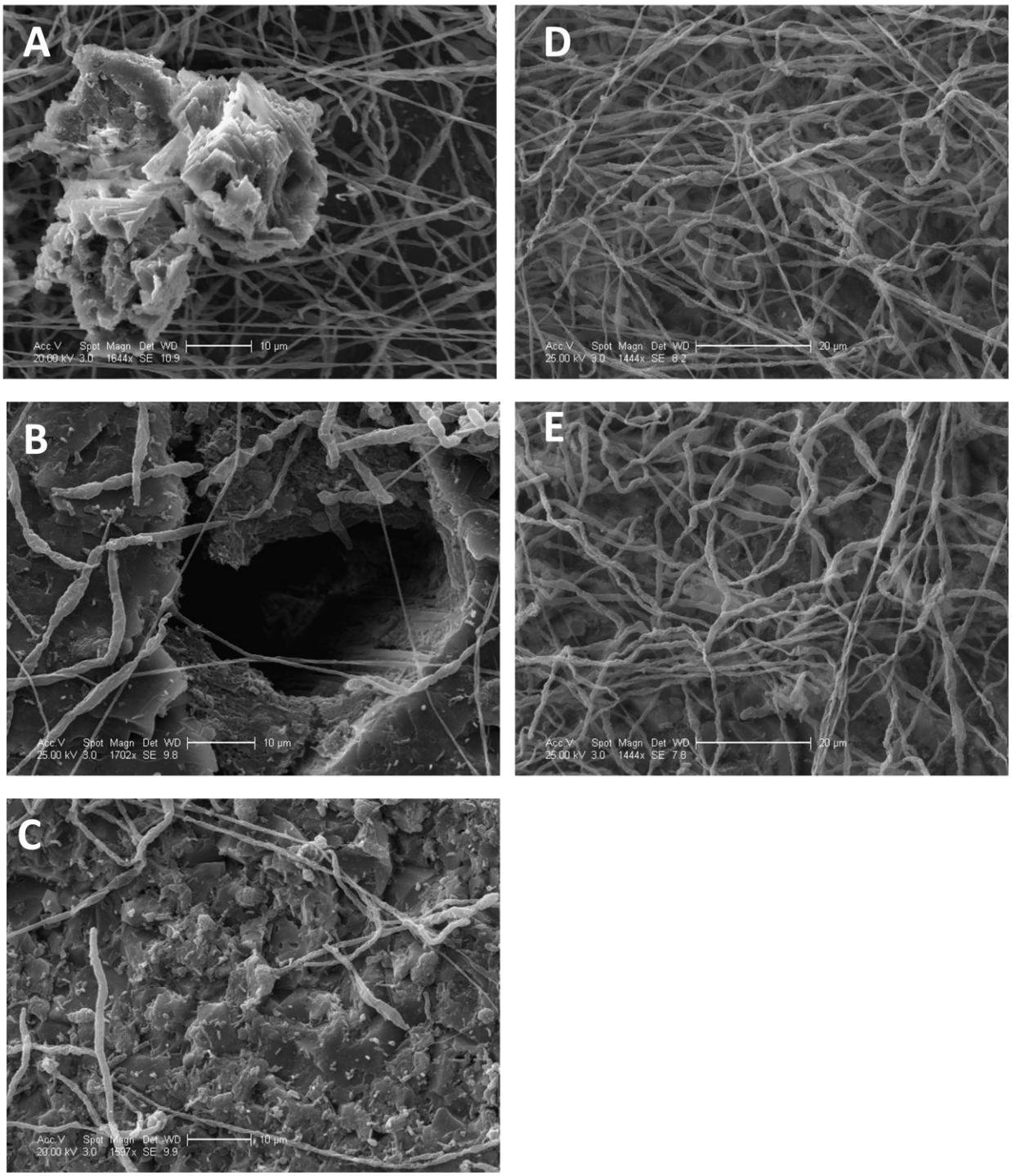

Figure 11. SEM images of silicate coupons retrieved from Biotic CDC 1 reactor inoculated with a pure culture of *Thiothrix unzii* performed at pH = 6.6 after 3 weeks in reactor. A is Kspar, B is Albite, C is Chert, D is Basalt, E is Quartz. Scale bar is 10 μm for A, B, & C; 20 μm for D & E.

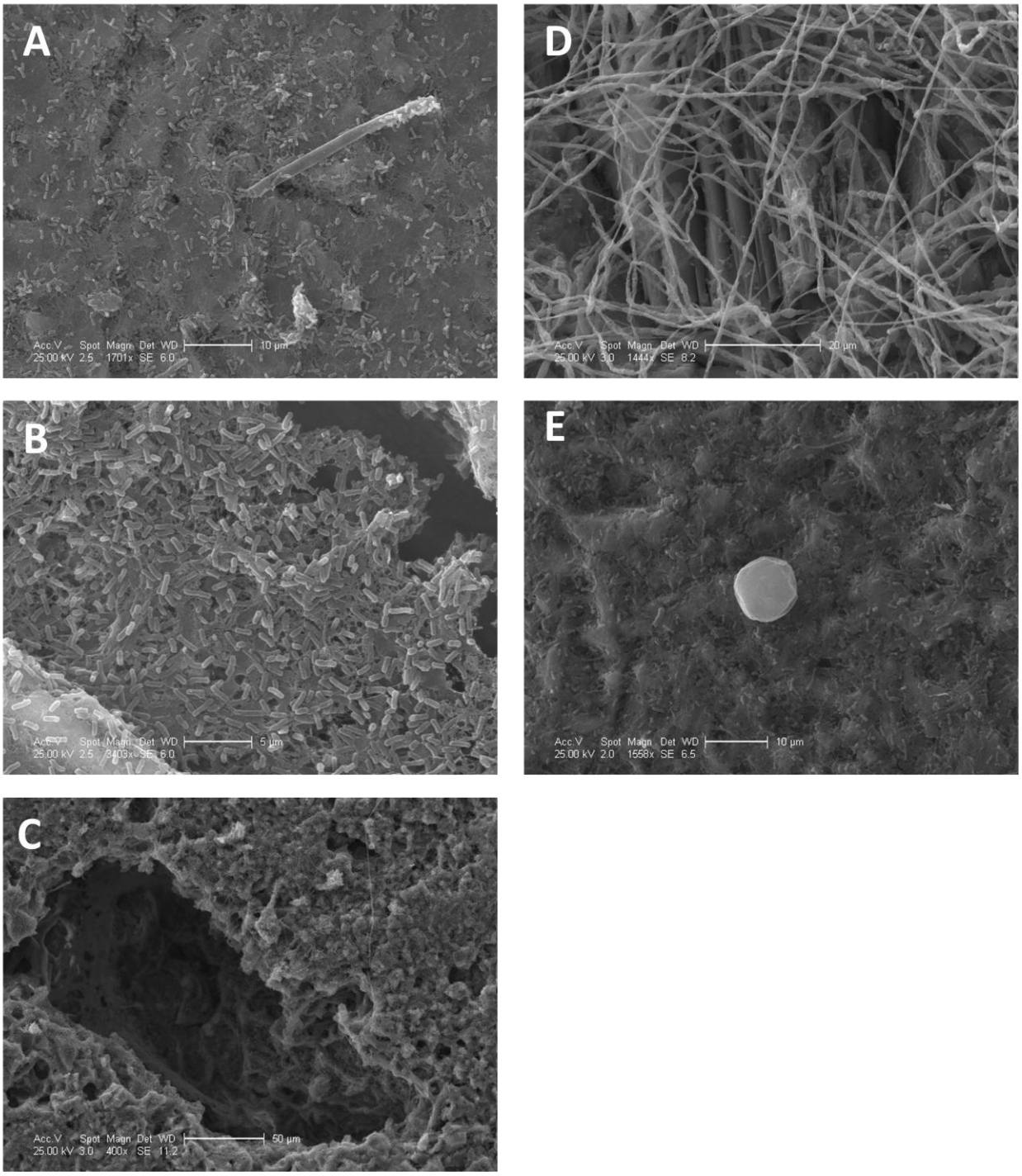

Figure 12. SEM images of silicate coupons retrieved from Biotic CDC 2 reactor inoculated with a LKC microbial mat performed at pH = 6.6 after 3 weeks in reactor. A is Kspar, B is Albite, C is Chert, D is Basalt, E is Quartz. Scale bars vary: A is 10 μm, B is 5 μm, C is 50 μm, D is 20 μm, E is 10 μm. Note the abundant filaments on basalt (D).

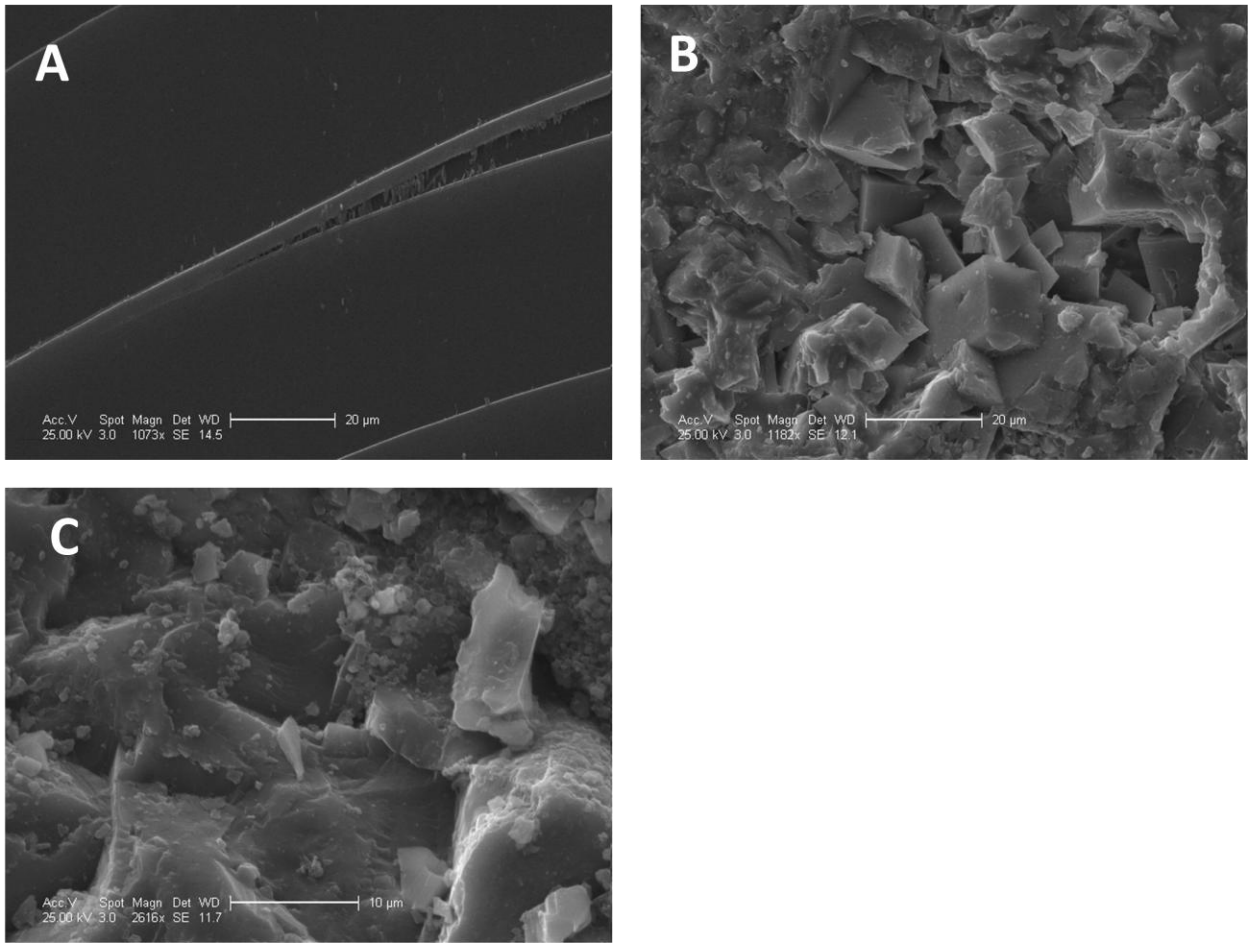

Figure 13. SEM images of carbonate coupons that were not run in the CDC reactor. A is Iceland Spar, B is Limestone, C is Dolostone. Scale bar is 20 μm on A and B, 10 μm on C. Coupons surfaces are free of corrosive textures.

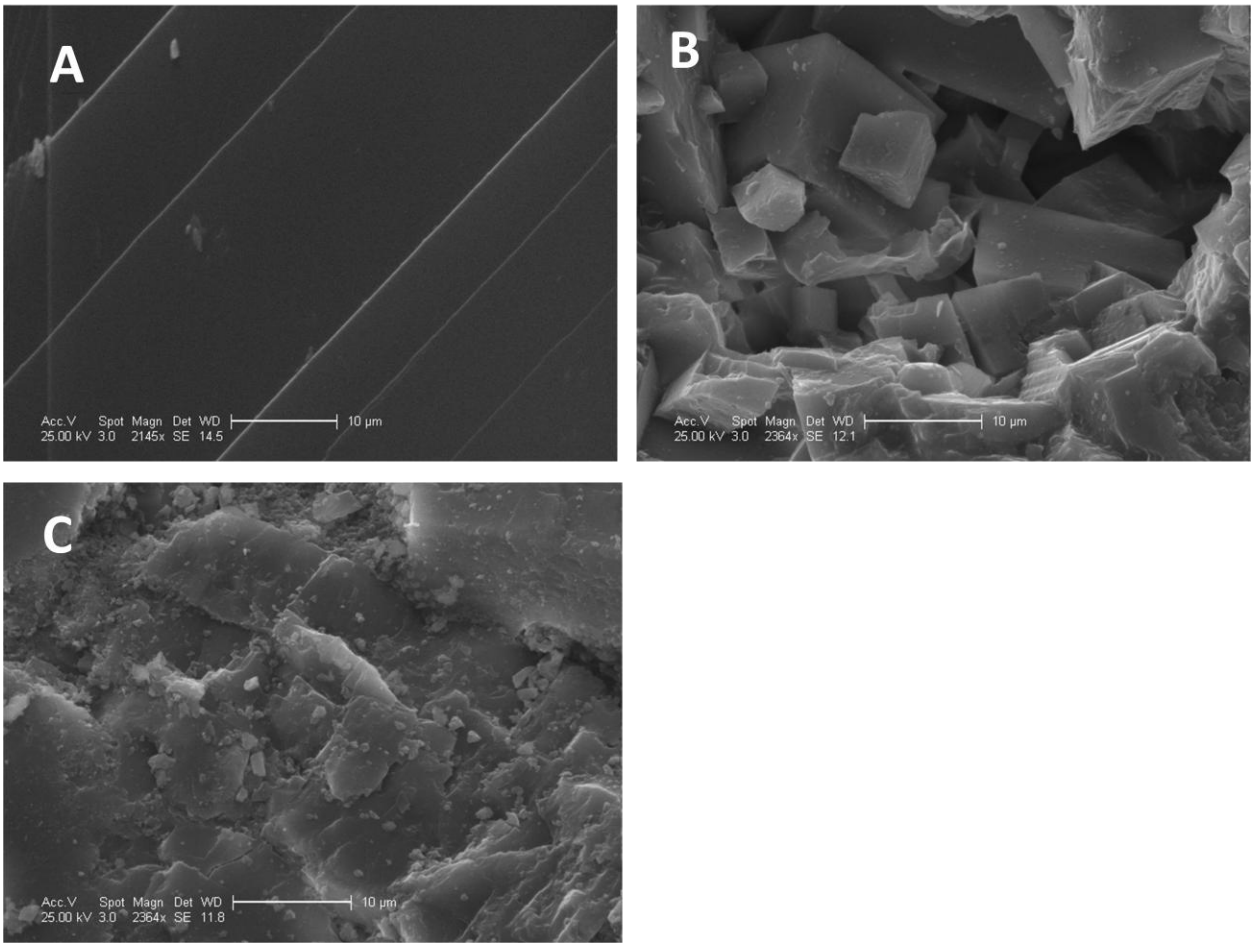

Figure 14. SEM images of carbonate coupons retrieved from Abiotic CDC reactor performed at pH = 6.6 after 3 weeks in reactor. A is Iceland spar calcite, B is Limestone, C is Dolostone. Scale bar is 10 μm. Coupon surfaces are free of corrosive textures.

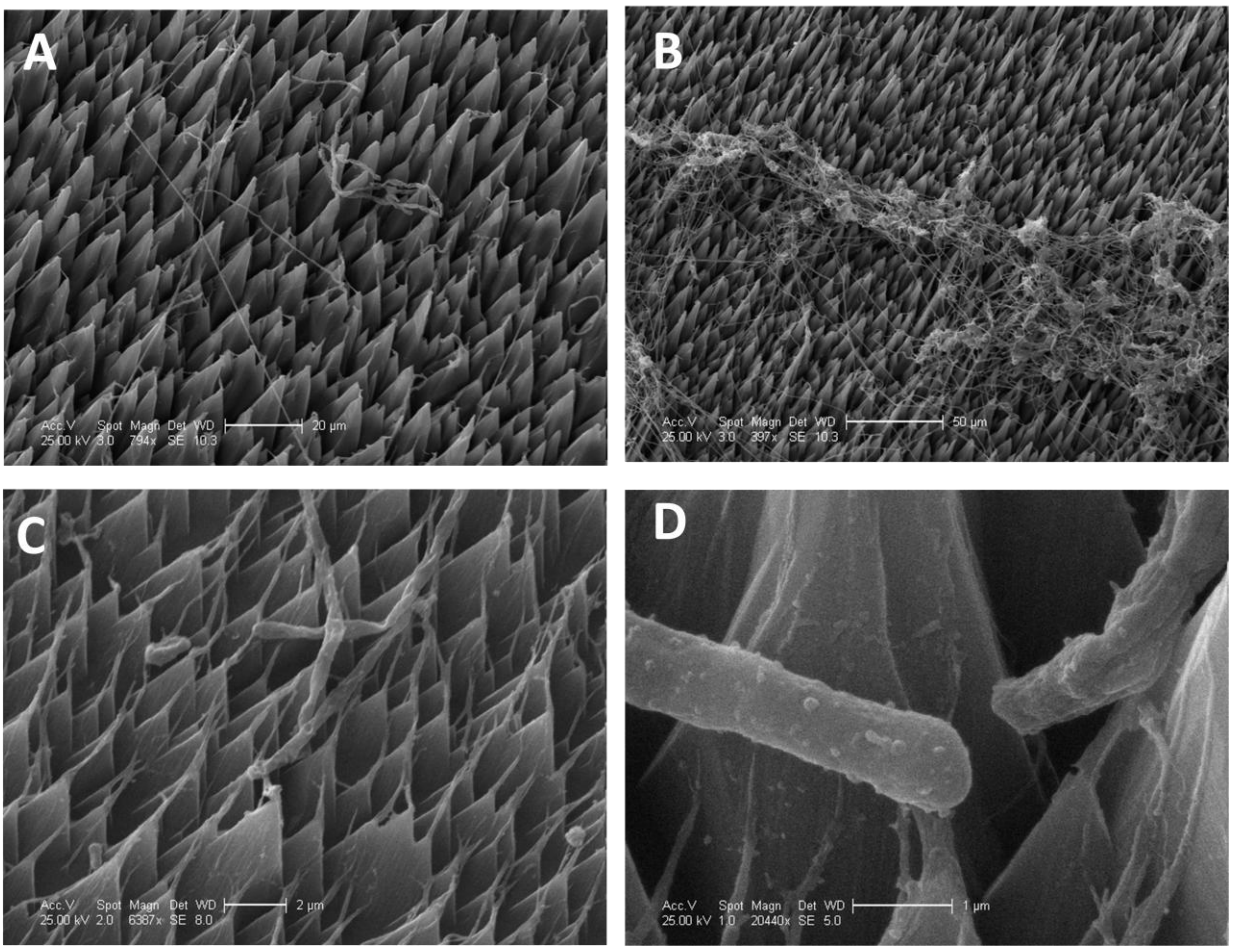

Figure 15. SEM images of Iceland spar calcite coupons retrieved from Biotic CDC 1 reactor inoculated with a pure culture of *Thiothrix unzii* at pH = 6.6 after 3 weeks in reactor. Scale bars are; A:20 μm, B:50 μm, C:2 μm, D:1 μm. Spiky texture is evidence of microbial corrosion of calcite. Each individual spike is coated with EPS.

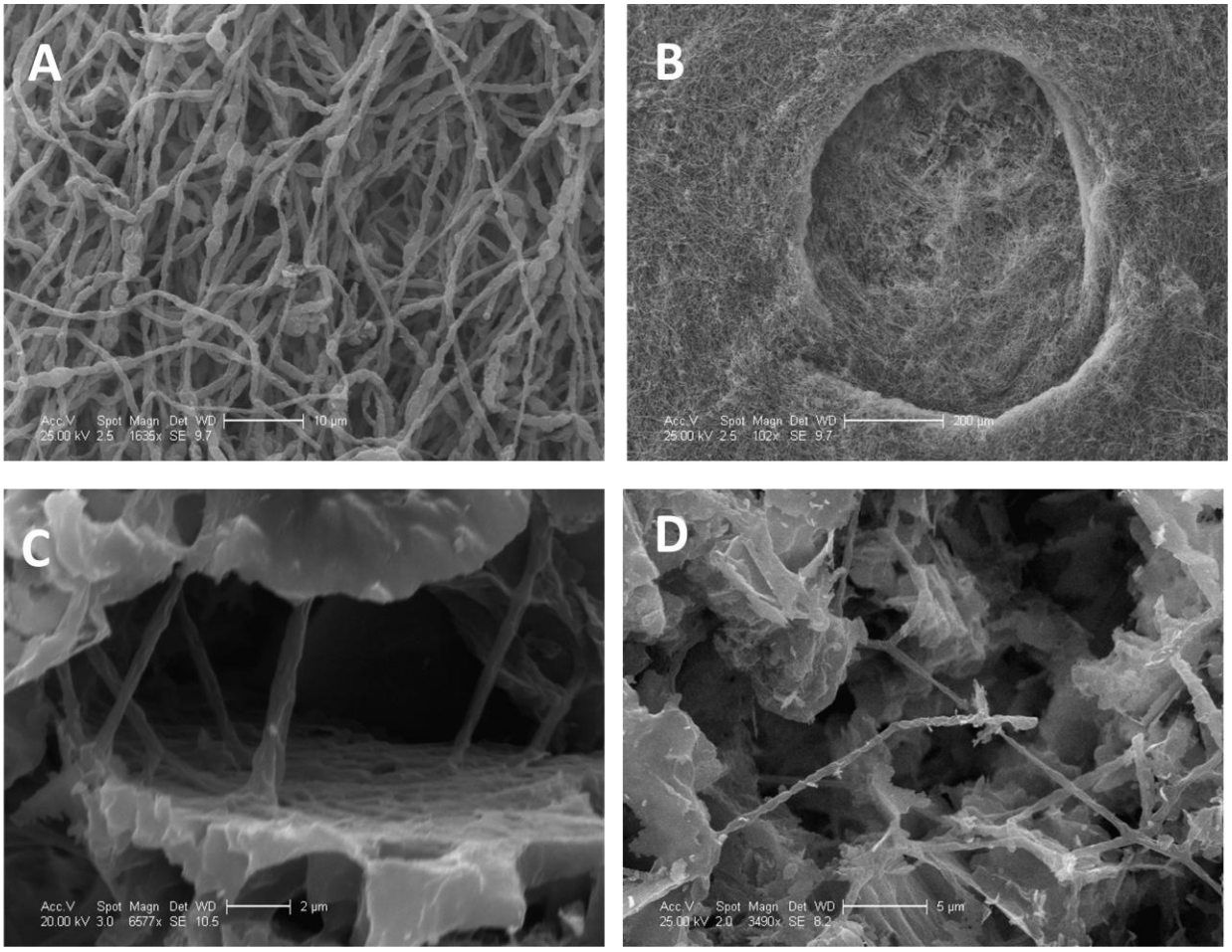

Figure 16. SEM images of Limestone (A,B) and Dolostone (C,D) retrieved from Biotic CDC 1 reactor inoculated with a pure culture of *Thiothrix unzii* at pH = 6.6 after 3 weeks in reactor. Scale bars are; A:10 μm, B:200 μm, C:2 μm, D:5 μm. Filaments are abundant and surface coverage is nearly total.

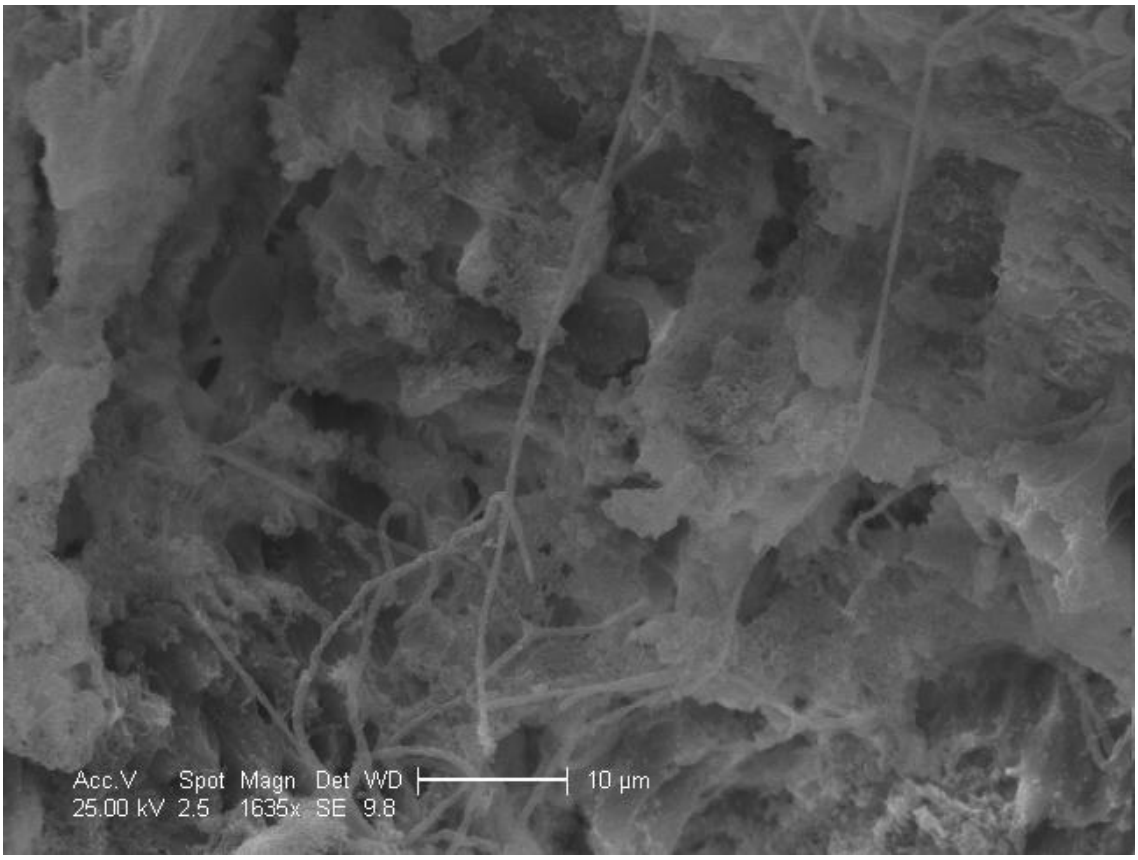

Figure 17. SEM images of Madison Limestone retrieved from Biotic CDC 1 reactor inoculated with a pure culture of *Thiothrix unzii* at pH = 6.6 after 3 weeks in reactor. Scale bar is 10 μm. Microbial corrosion textures are evident.

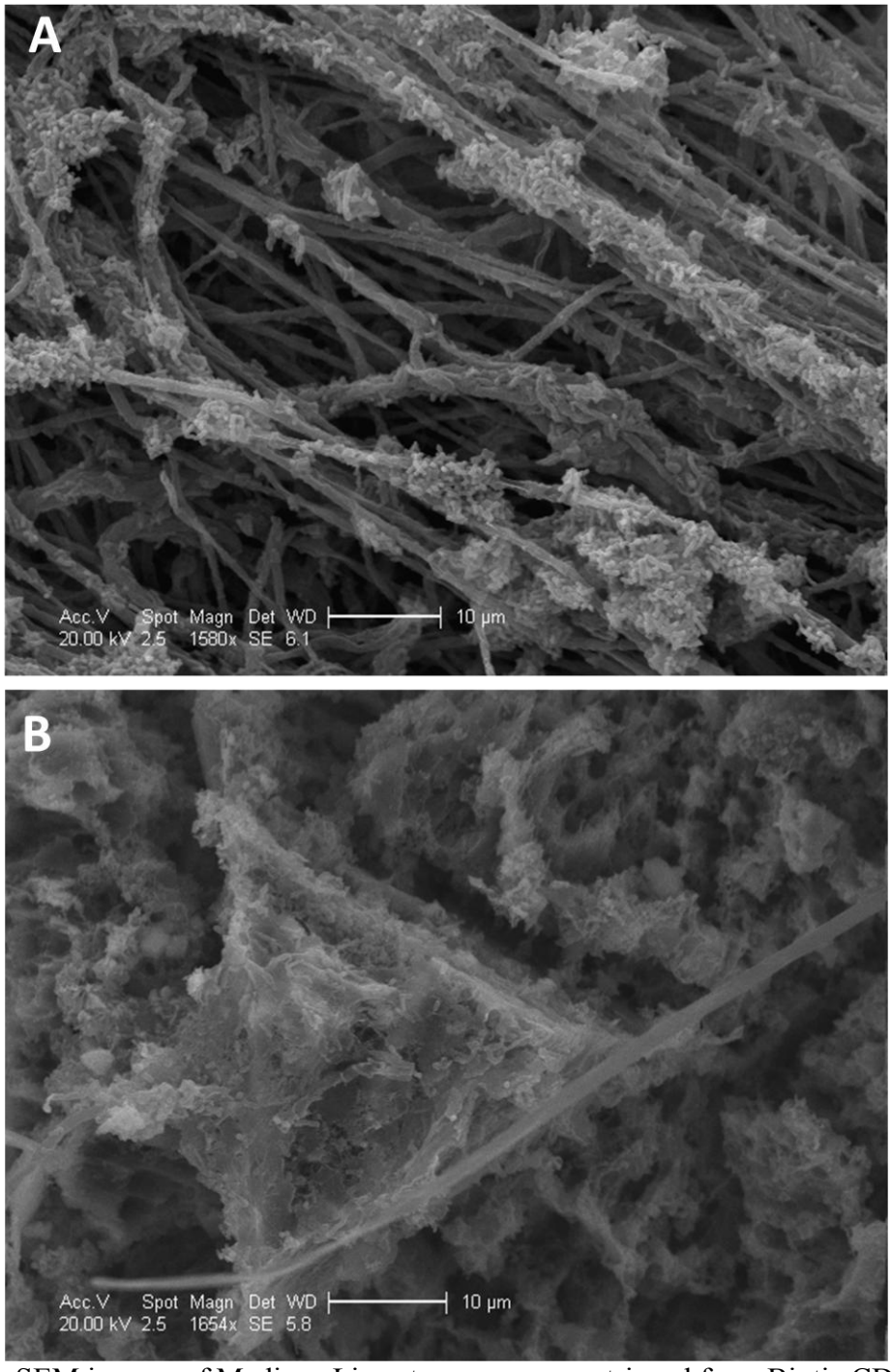

Figure 18. SEM images of Madison Limestone coupons retrieved from Biotic CDC 2 reactor inoculated with a LKC microbial mat at pH = 6.6 after 3 weeks in reactor. (A) is raw with biofilm preserved, (B) is after partial biofilm removal. Scale bars are 10 μm. Sub-biofilm corrosion textures are visible in 18B.

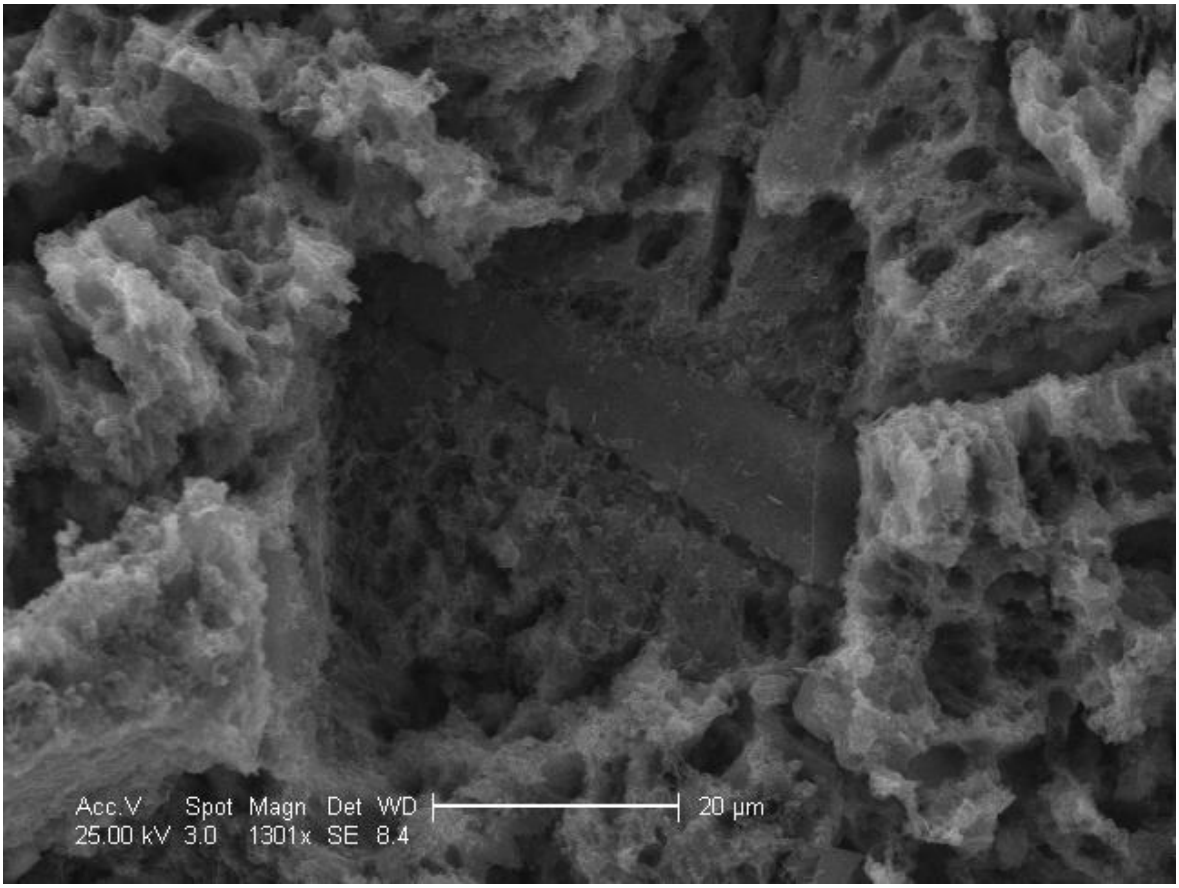

Figure 19. SEM images of Dolostone coupon retrieved from Biotic CDC 2 reactor inoculated with a LKC microbial mat at pH = 6.6 after 3 weeks in reactor. Scale bar is 20 μm. Sub-biofilm corrosion textures are evident.

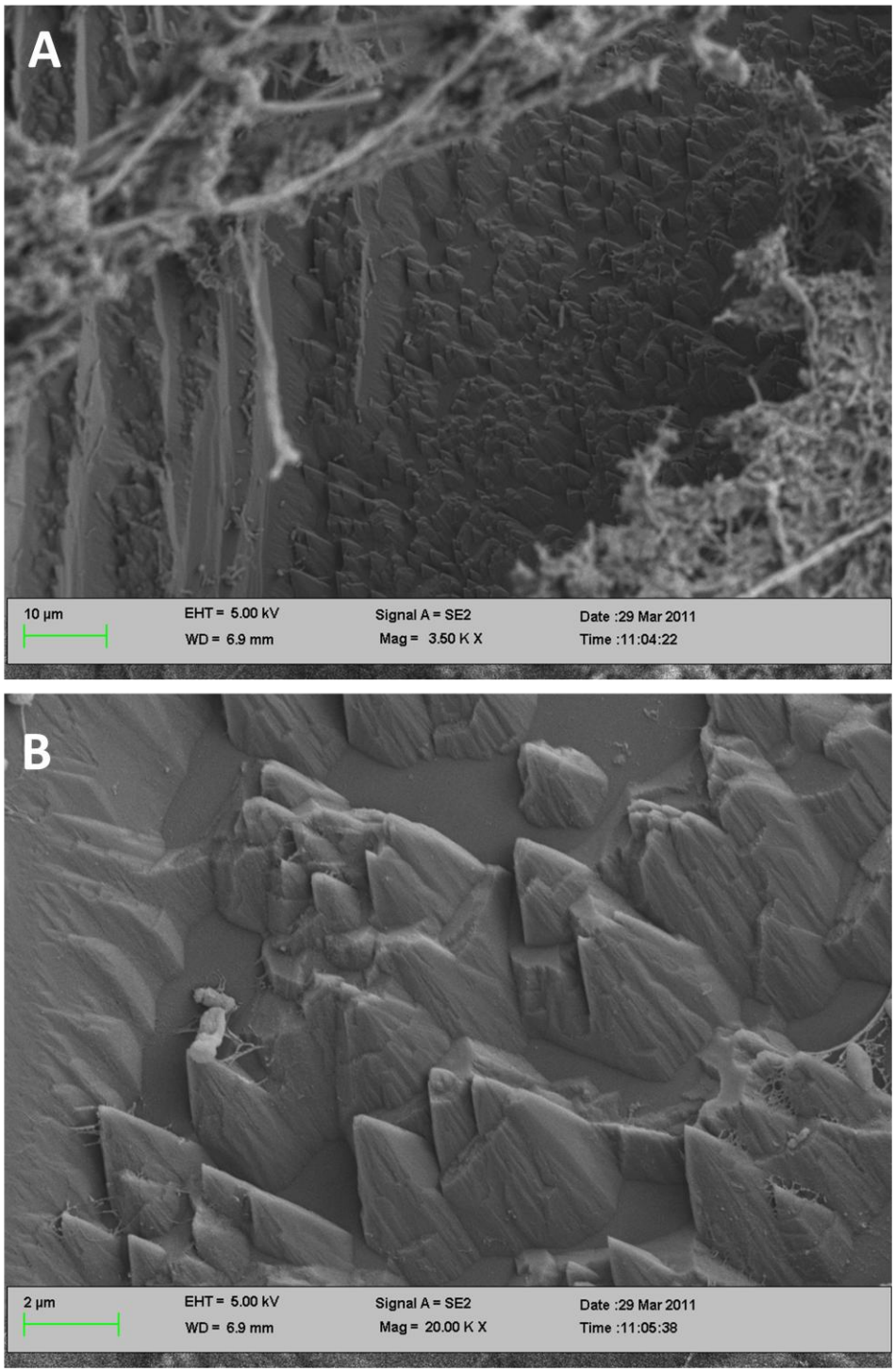

Figure 20. SEM images of Iceland Spar coupons retrieved from Biotic CDC 4 reactor inoculated with a LKC microbial mat performed at pH = 8.3 after 3 weeks in reactor. A scale bar 10 μm, B scale bar 2 μm. Spiky surface corrosion textures are similar to those in pure culture experiments (Figure 15).

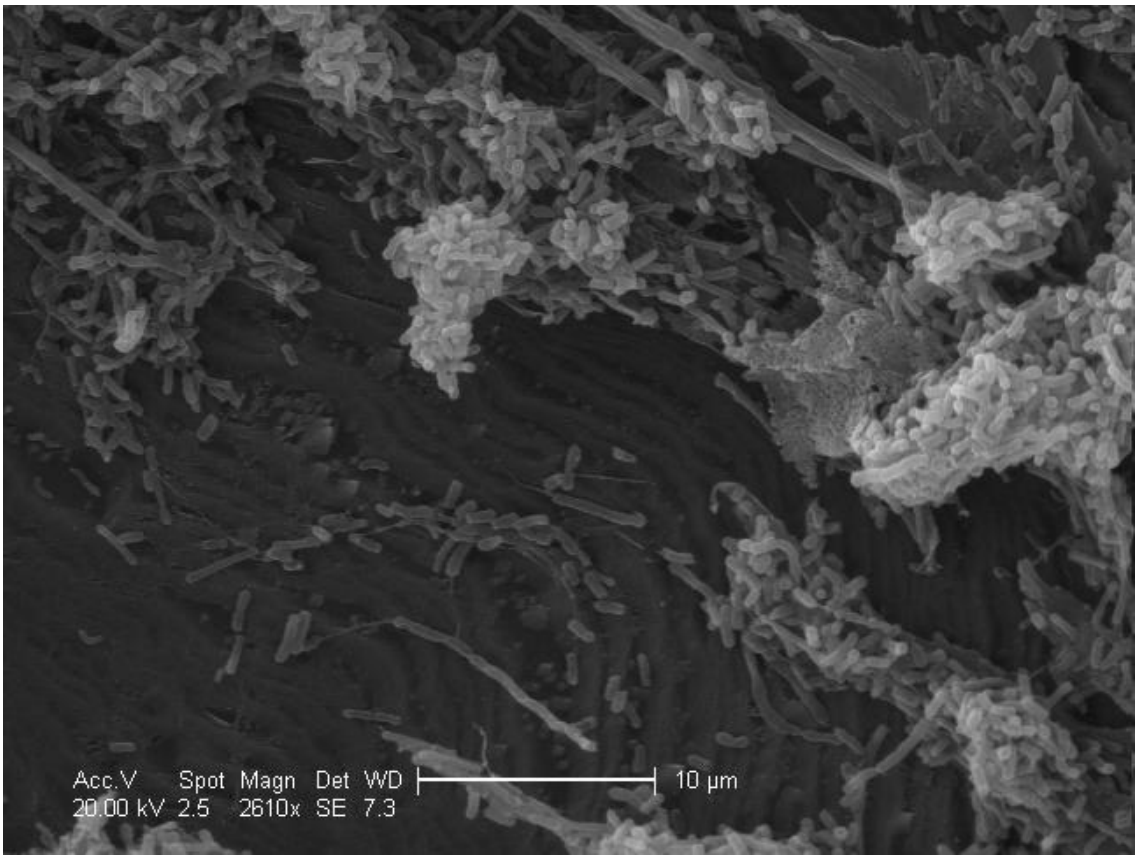

Figure 21. SEM image of Iceland Spar coupon retrieved from Biotic CDC 4 reactor inoculated with a LKC microbial mat performed at pH = 8.3 after 3 weeks in reactor. Scale bar 10 μm. Bulk media was at equilibrium w.r.t. calcite which resulted in corrosive textures that resemble filamentous morphologies.

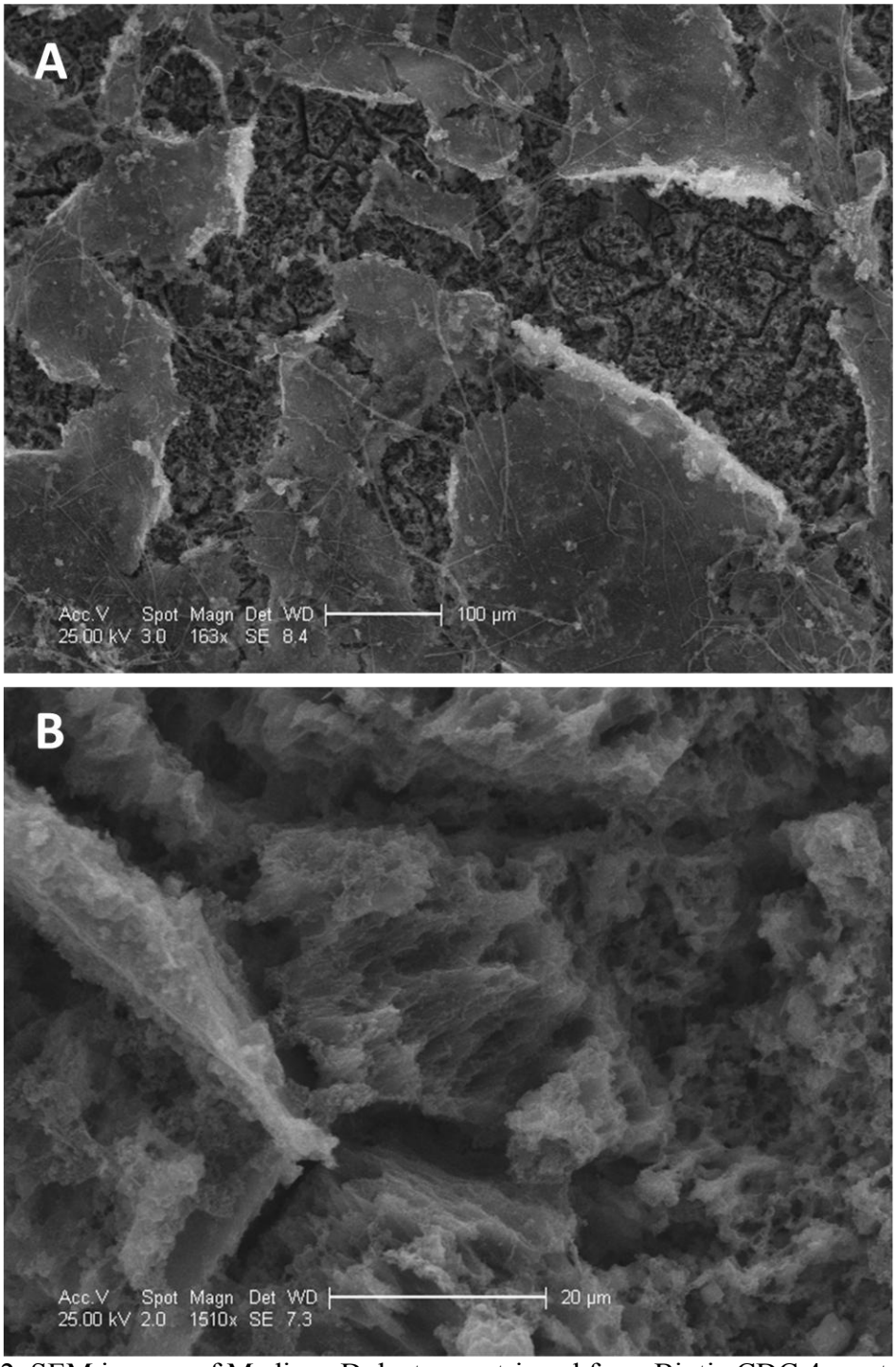

Figure 22. SEM images of Madison Dolostone retrieved from Biotic CDC 4 reactor inoculated with a LKC microbial mat performed at pH = 8.3 after 3 weeks in reactor. Scale bars; (A) 100 μm, (B) 20 μm. Bulk media was at equilibrium w.r.t. calcite. However sub-biofilm corrosion is still evident.

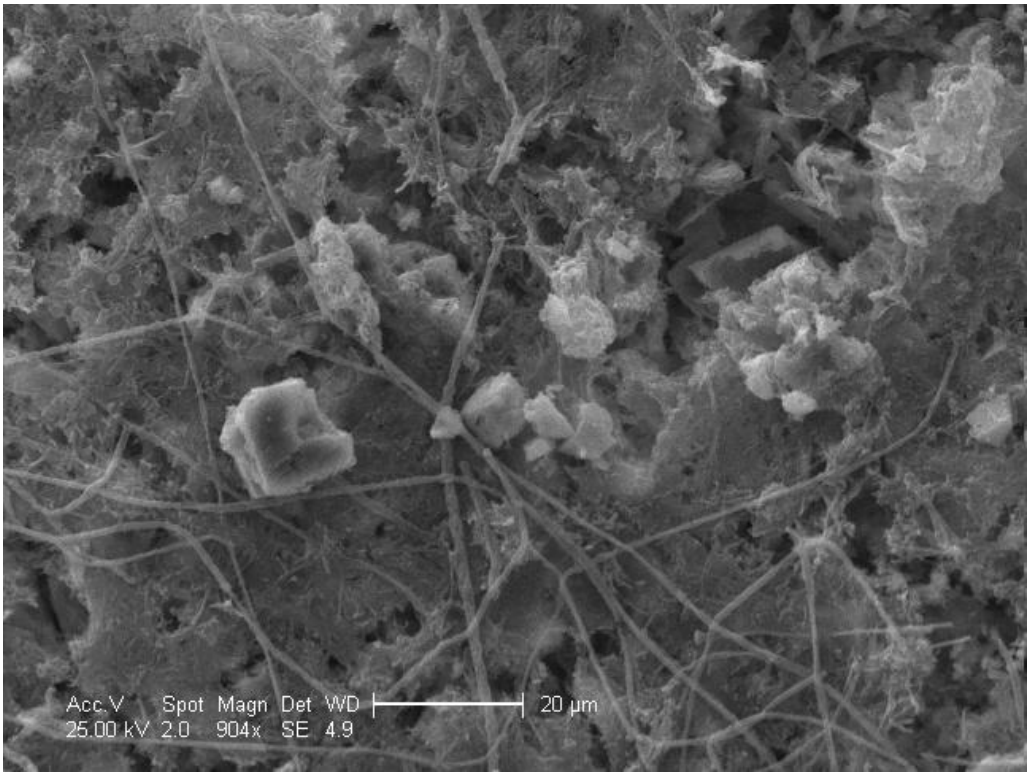

Figure 23. SEM image of Madison Limestone Biofilm retrieved from Biotic CDC 4 reactor inoculated with a LKC microbial mat performed at pH = 8.3 after 3 weeks in reactor. Scale bar is 20 μm.

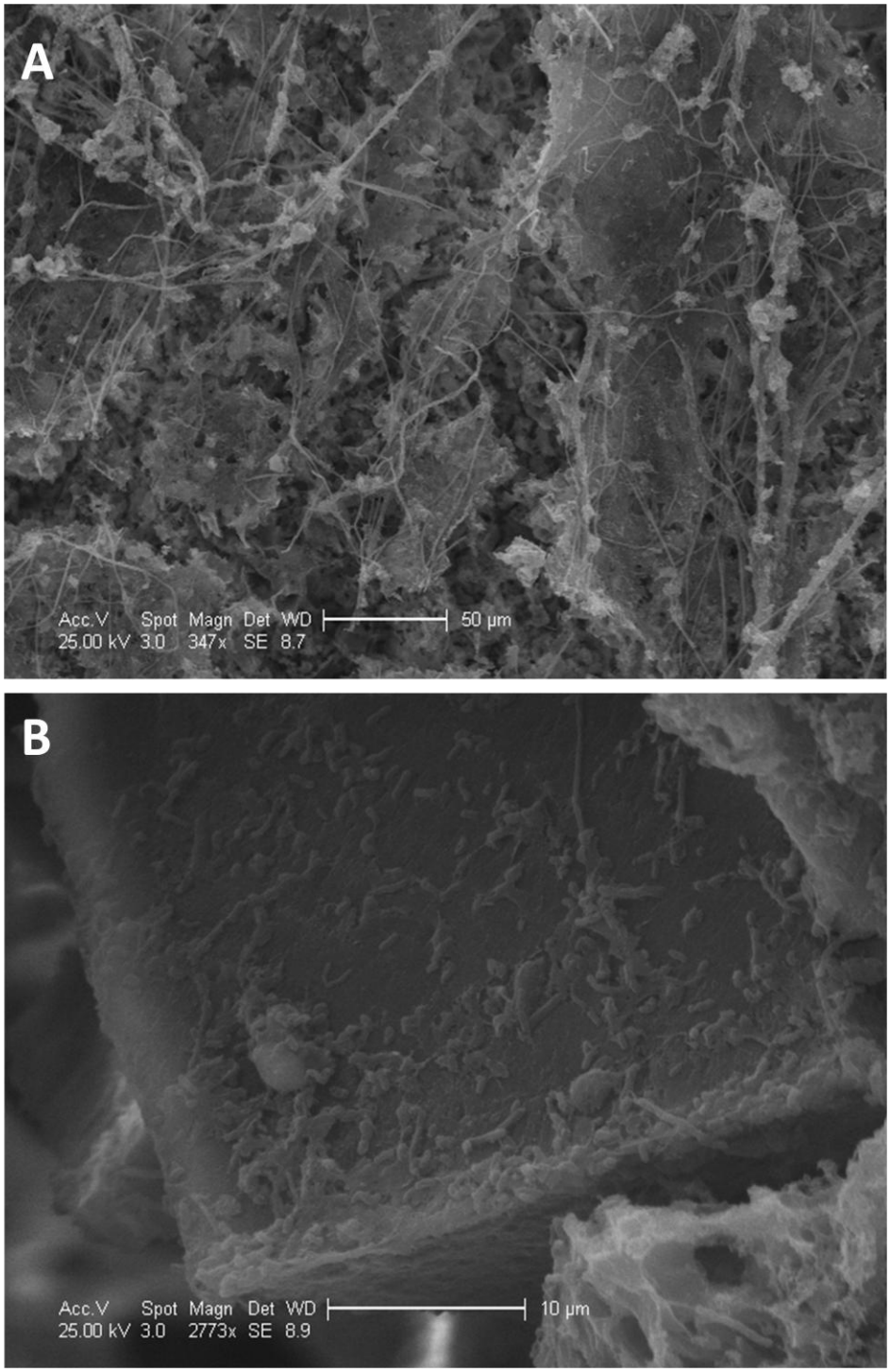

Figure 24. SEM images of Madison Limestone retrieved from Biotic CDC 4 reactor inoculated with a LKC microbial mat performed at pH = 8.3 after 3 weeks in reactor. Scale bars; (A) 50 μm, (B) 10 μm.

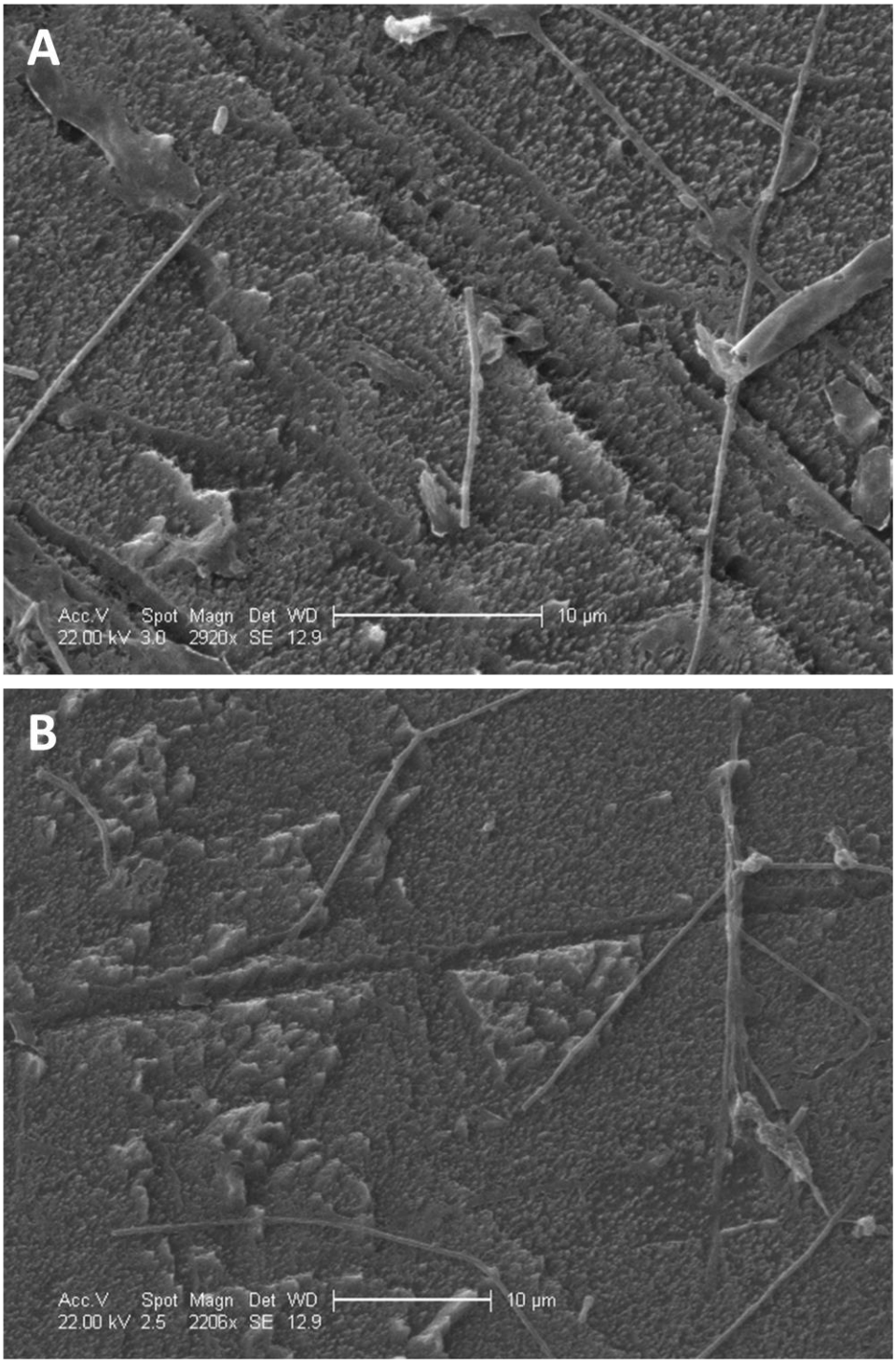

Figure 25. SEM images of Calcite from LKC CDC reactor inoculated with a LKC microbial mat performed within Lower Kane Cave, WY, USA after 1 week in a reactor. Scale bars are both 10 μm.

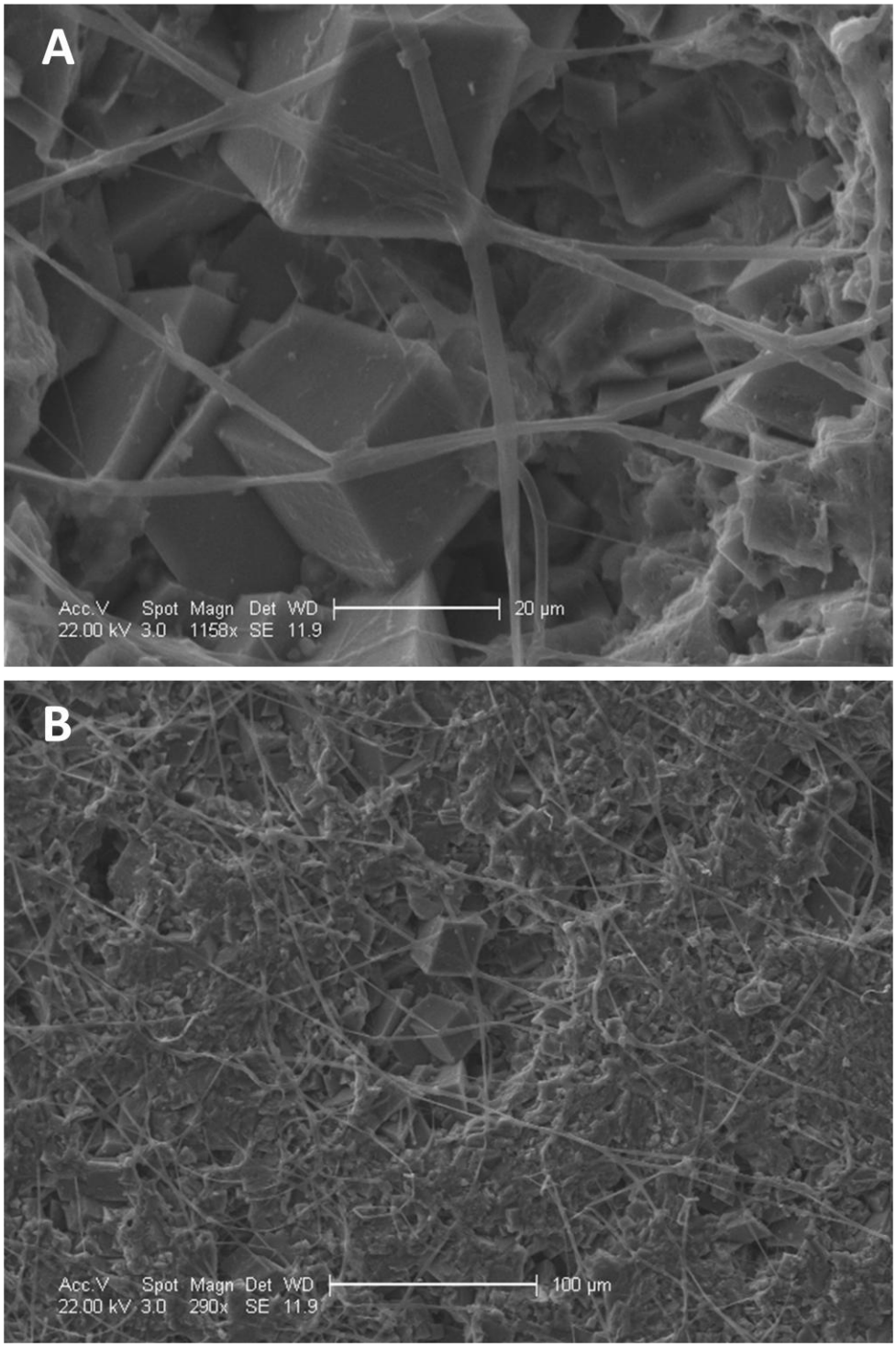

Figure 26. SEM images of Madison Limestone from LKC CDC reactor inoculated with a LKC microbial mat performed within Lower Kane Cave, WY, USA after 1 week in a reactor. Scale bars are; (A) 20 μm, (B) 100 μm.

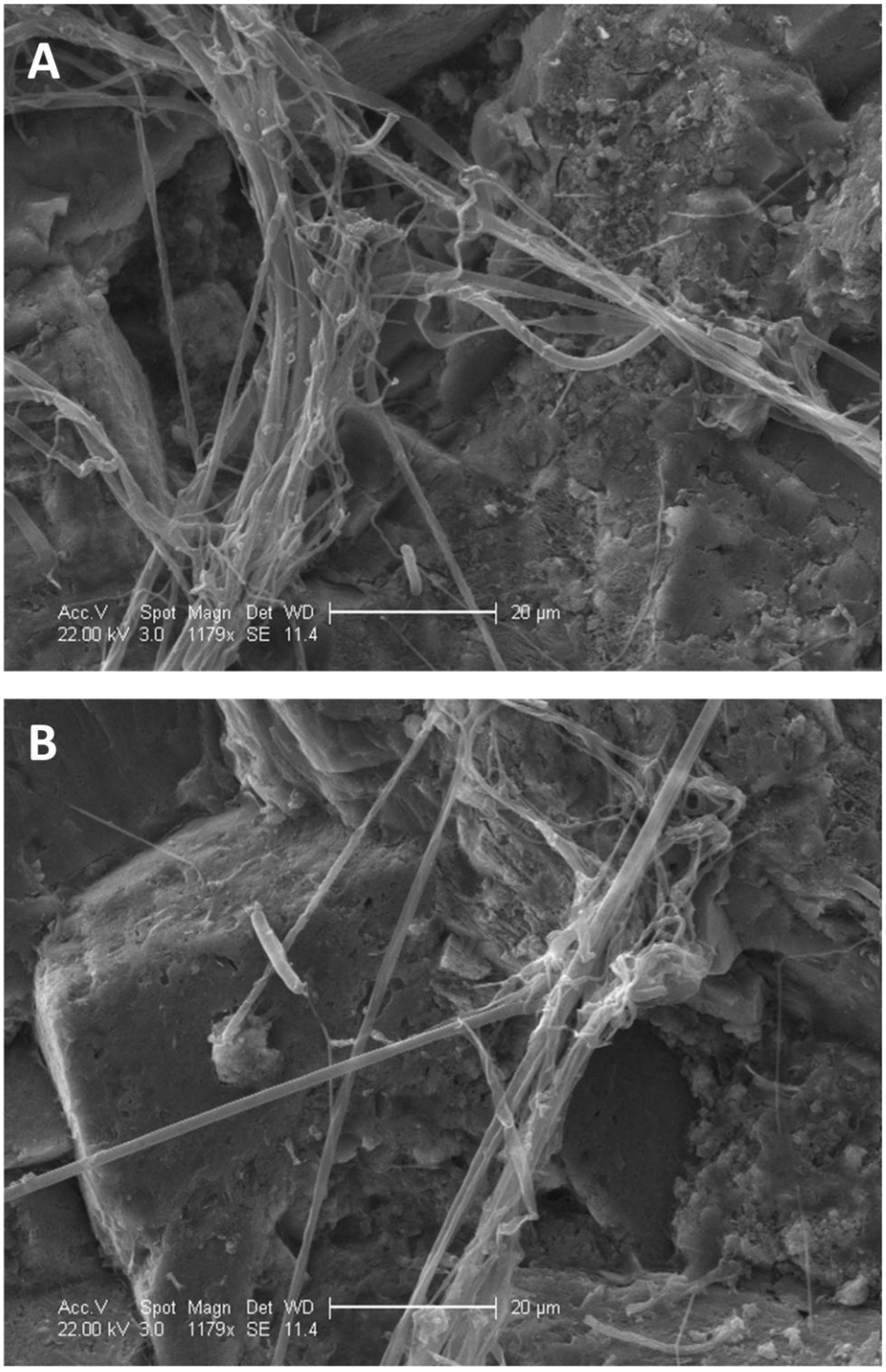

Figure 27. SEM images of Madison Dolostone from LKC CDC reactor inoculated with a LKC microbial mat performed within Lower Kane Cave, WY, USA after 1 week in a reactor. Scale bars are both 20 μm.

REFERENCES

Appelo, C.A.J.. and Postma, D., (2007), Geochemistry, groundwater and pollution. 2nd edition. A.A. Balkema Publishers. 2007.

Banfield, J.F., Barker, W.W., Welch, S.A., Taunton, A., (1999), Biological impact on mineral dissolution: Application of the lichen model to understanding mineral dissolution in the rhizosphere: Proceedings of the National Academy of Sciences USA, 1999;96, p. 3404-3411 doi: 10.1073/pnas.96.7.3403.

Barton, H., Luiszer, F., (2005), Microbial metabolic structure in a sulfidic cave hot spring: Potential mechanisms of biospeleogenesis. Journal of Cave and Karst Studies. V. 67, No. 1, P. 28-38.

Bennett, P.C., Hiebert, F.K., and Rogers, J.R., (2000), Microbial control of mineral-groundwater equilibria - macroscale to microscale: Hydrogeology Journal, v. In Press.

Bennett, P.C., Rogers, J.R., Hiebert, F.K., Choi,W.J., (2001), Silicates, silicate weathering, and microbial ecology. Geomicrobiol. J. 18, 3 –19.

Bennett, P.C., Summers-Engel, A., (2006), NSF.

Burlage, R.S., Atlas, R., Stahl, D., Geesey, G., Sayler, G., (1998), Techniques in Microbial Ecology. Oxford University Press.

Buhmann, D., and Dreybrodt, W., (1985), The kinetics of calcite dissolution and precipitation in geologically relevant situations of karst areas; 1, Open system: Chemical Geology, v. 48, p. 189-211.

Campbell B.J., A.S. Engel, M.L. Porter, and K. Takai. (2006). The versatile εproteobacteria: Key players in sulphidic habitats. *Nature Reviews Microbiology* 4:458–468.

Cubillas, P., Köhler, S., Prieto, M., Chaïrat, C., and Oelkers, E.H., (2005), Experimental determination of the dissolution rates of calcite, aragonite, and bivalves: Chemical Geology, v. 216, p. 59-77.

Davis, K.J., Nealson, K.H., and Luttge, A., (2007), Calcite and dolomite dissolution rates in the context of microbe-mineral surface interactions: Geobiology, V. 5, P. 191-205.

Dreybrodt, W., (1981), Kinetics of the dissolution of calcite and its applications to karstification: Chemical Geology, v. 31, p. 245-269.

Dreybrodt, W., (1987), The kinetics of calcite dissolution and its consequences to karst evolution from the initial to the mature state: NSS Bulletin, v. 49, p. 31-49.

Dreybrodt, W., Eisenlohr, B.M., Ringer, S., (1997). Precipitation kinetics of calcite in the system CaCO3-H2O-CO2: The conversion to CO2 by the slow process H+ + HCO3- → CO2 + H2O as a rate limiting step. Geochimica et Cosmochimica Acta, Vol. 61, No. 18, pp. 3897-3904., 1997

Eaton, A.D., Clesceri, L.S., Rice, E.W., Greenberg, A., and (2005). Standard methods for the examination of water and wastewater, 21st. ed. American Public Health Association, Washington, D.C., Pp. 4-183-184.

Egemeier, S., (1981), Cave development by thermal waters: National Speleological Society Bulletin, v. 43, p. 31-51.

Ehrlich, H.L., (1996), How microbes influence mineral growth and dissolution: Chemical Geology, v. 132, p.5-9.

Engel, A.S., Porter, M.L., Kinkle, B.K., and Kane, T.C., (2001), Ecological assessment and geological significance of microbial communities from Cesspool Cave, Virginia: Geomicrobiology journal, v. 18, p. 259-274.

Engel, A.S., Lee, N., Porter, M.L., Stern, L.A., Bennett, P.C., and Wagner, M., (2003), Filamentous "*Epsilonproteobacteria*" dominate microbial mats from sulfidic cave springs: Applied and Environmental Microbiology, v. 69.

Engel, A.S., Stern, L.A., and Bennett, P.C., (2004), Microbial contributions to cave formation: new insight into sulfuric acid speleogenesis: Geology, v. 32, p. 369-372.

Ford, D., and Williams, P., (1989), Karst Geomorphology and Hydrology: London, Unwin Hyman, 601

Franson, M.A., (1975), Standard Methods for the Examination of Water and Wastewater: Washington, DC, American Public Health Association.

Hill, T.C.J., Walsh, K.A., Harris, J.A., and Moffett, B.F., (2003), Using ecological diversity measures with bacterial communities: FEMS Microbiology Ecology, v. 43, p. 1-11.

Hose, L.D., Palmer, A.N., Palmer, M.V., Northup, D.E., Boston, P.J., and DuChene, H.R., (2000), Microbiology and geochemistry in a hydrogen-sulphide rich karst environment: Chem. Geol., v. 169, p. 399-423.

Howarth, R., Unz, R.F., Seviour, E.M., Seviour, R.J., Blackall, L.L., Pickup, R.W., Jones, J.G., Yaguchi, J., and Head, I.M., (1999), Phylogenetic relationships of filamentous sulfur bacteria (*Thiothrix* spp. and Eikelboom type 021N bacteria) isolated from wastewater-treatment plants and description of *Thiothrix eikelboomii* sp. nov., *Thiothrix unzii* sp. nov., *Thiothrix fructosivorans* sp. nov. and *Thiothrix defluvii* sp. nov.: International Journal of Systematic Bacteriology, v. 49, p. 1817-1827.

Huber, J.A., Welch, D.B.M., Morrison, H.G., Huse, S.M., Neal, P.R., Butterfield, D.A., Sogin, M.C., (2007), Microbial population structures in the deep marine biosphere. Science. V. 318, no. 5847, p. 97-100.

Jansson, M., (1987), Anaerobic dissolution of iron-phosphorus complexes in sediment due to the activity of nitrate-reducing bacteria: Microbial Ecology, V. 14, p. 81-89, DOI 10.1007BF02011573

Jeschke, A.A., and Dreybrodt, W., (2002), Dissolution rates of minerals and their relation to surface morphology: Geochimica et Cosmochimica Acta, v. 66, p. 3055-3062.

Jones, D.S., Lyon, E.H., and Macalady, J.L., (2008), Geomicrobiology of sulfidic cave biovermiculations. Journal of Cave and Karst (in press).

Kelly DP (1982) Biochemistry of the chemolithotrophic oxidation of inorganic sulphur. Philos Trans R Soc Lond Biol 298:499–528

Kelly DP (1988) Oxidation of sulphur compounds. Soc Gen Microbiol Symp 42:65–98

Kelly DP (1990) Energetics of chemolithotrophs. In: Krulwich TA (ed) Bacterial energetics. Academic Press, San Diego, pp 479–503

Kelly, D.P., (1999), Thermodynamic aspects of energy conservation by chemolithotrophic sulfur bacteria in relation to the sulfur oxidation pathways: Archives of Microbiology, v. 171, p. 219-229.

Kelly, D.P., Wood, A.P., (2000), Reclassification of some species of *Thiobacillus* to the newly designated genera *Acidithiobacillus* gen. nov., *Halothiobacillus* gen. nov. and *Thermithiobacillus* gen. nov. International Journal of Systematic and Evolutionary Microbiology (2000), v. 50, pp 511–516.

Lane DJ. (1991), 16S/23S rRNA Sequencing. In: Stackebrandt E and Goodfellow M (eds) Nucleic Acid Techniques in Bacterial Systematics. John Wiley & Sons: New York, USA, pp 115-147.

Liu, Z., and Dreybrodt, W., (1997), Dissolution kinetics of calcium carbonate minerals in H2O-CO2 solutions in turbulent flow: The role of the diffusion boundary layer and the slow reaction H2O + CO2 --> H+ + HCO3-: Geochimica et Cosmochimica Acta, v. 61, p. 2879-2889.

Mabin, K., (2005), Transport and transformation of sulfur species during sulfuric acid speleogenesis: Geomicrobiological sulfur cycling within Lower Kane Cave, Wyoming: Austin, The University of Texas at Austin.

Macalady, J.L., Jones, D.S., Lyon, E.H., (2007), Extremely acidic, pendulous cave wall biofilms from Frasassi cave system, Italy: Environmental Microbiology, v.9(6), p. 1402-1414.

Magurran, A. E. (1988). *Ecological diversity and its measurement.* Princeton University Press, Princeton, N. J.

Magurran, A. E. (2004). *Measuring biological diversity*. Blackwell.

Millero, F.J., Hubinger, S., Fernandez, M., and Garnett, S., (1987), Oxidation of H2S in seawater as a function of temperature, pH, and ionic strength: Environmental Science and Technology, v. 21, p. 439-443.

Morse, J.W., and Berner, R.A., (1974), The dissolution kinetics of calcite.

Morse, J.W., (1983), The kinetics of calcium carbonate dissolution and precipitation: Reviews in Mineralogy, v. 11, p. 227-264.

Morse JW, Mackenzie FT (1990) Geochemistry of Sedimentary Carbonates. Elsevier, Amsterdam

Morse, J.W., and Arvidson, R.S., (2002), The dissolution kinetics of major sedimentary carbonate minerals: Earth-Science Reviews, v. 58, p. 51-84.

Norris, P.R., Davis-Belmar, C.S., Brown, C.F., Calvo-Bado, L.A., (2011), Autotrophic, sulfur-oxidizing actinobacteria in acidic environments: Extremophiles (2011). 15, pp 155–163.

Paine SG, Lingood FV, Schimmer F, Thrupp TC (1933) IV. The relationship of microorganisms to the decay of stone: Philosophical Transactions of the Royal Society of London, Series B, Biological Sciences 222B, p. 97–127.

Pearson, M.E., (2004), Geochemical and isotopic tracing of Paleozoic groundwater flow in breached anticlines: A case study at Lower Kane Cave, Big Horn Basin, Wyoming. Thesis. The University of Texas at Austin. Master of Science in Geological Sciences.

Peterson, J.A., (1984), Stratigraphy and sedimentary facies of the Madison Limestone and associated rocks in parts of Montana, Nebraska, North Dakota, South Dakota, and Wyoming. Washington, DC: Geological Survey Professional Paper 1273-A. 34 P.

Plummer, L.N., Wigley, T.M.L., and Parkhurst, D.L., (1978), The kinetics of calcite dissolution in CO (sub 2) -water systems at 5 degrees to 60 degrees C and 0.0 to 1.0 atm CO (sub 2): American Journal of Science, v. 278, p. 179-216.

Rogers, J.R., Bennett, P.C., (2004), Mineral stimulation of subsurface microorganisms: release of limiting nutrients from silicates: Chemical Geology, Volume 203, Issues 1-2, 15 January 2004, Pages 91-108.

Sievert, S.M., Kiene, R.P., Schulz-Vogt, H.N., (2007), The sulfur cycle. Oceanography, v. 20, No. 2.

Sjoeberg, E.L., and Rickard, D.T., (1984), The influence of experimental design on the rate of calcite dissolution: Geochimica et Cosmochimica Acta, v. 47, p. 2281-2285.

Steinhauer, E.S., (2008), Microbial influence on the kinetics of karstification: Austin, University of Texas at Austin, M.S. Thesis.

Steinhauer, Elspeth S., Omelon, Christopher R. and Bennett, Philip C.,(2010) 'Limestone Corrosion by Neutrophilic Sulfur-Oxidizing Bacteria: A Coupled Microbe-Mineral System', Geomicrobiology Journal, 27: 8, 723 — 738

Stock, G.M., Riihimaki, C.A., and Anderson, R.S., (2006), Age constraints on cave development and landscape evolution in the Bighorn Basin of Wyoming, USA. *Journal of Cave and Karst Studies*, v. 68, no. 2, p. 76–84.

Strohl, W.R., and Schmidt, T.M., (1984), Mixotrophy of the colorless, sulfide-oxidizing, gliding bacteria Beggiatoa and Thiothrix, *in* Sprott, G.D., and Jarrell, K.F., eds., Electrochemical Potential and Membrane Properties of Methanogenic Bacteria: Columbus, Ohio State Press, p. 79-95.

Thamdrup, B., Finster, K., Hansen, J.W., and Bak, F., (1993), Bacterial disproportionation of elemental sulfur coupled to chemical reduction of iron or manganese: Applied and Environmental Microbiology, v. 59, p. 101-108.

Wolfaardt, G.M., Lawrence, J.R., Korber, D.R., (1999), Function of EPS. In: Wingender, J., Neu, T.R., Flemming, H-C, editors. Microbial extracellular polymeric substances: characterization, structure, and function New York: Springer. P 172–195.